Straddling the tholeiitic/calc-alkaline transition: the effects of modest amounts of water on magmatic differentiation at Newberry Volcano, Oregon

Citation: Mandler, Ben E., Julie M. Donnelly#Nolan, and Timothy L. Grove. "Straddling the tholeiitic/calc#alkaline transition: the effects of modest amounts of water on magmatic differentiation at Newberry Volcano, Oregon." Contributions to Mineralogy and Petrology. 2014 Oct 01;168(4):1066.

As Published: http://dx.doi.org/10.1007/s00410-014-1066-7

Publisher: Springer Berlin Heidelberg

Persistent URL: http://hdl.handle.net/1721.1/103549

Version: Author's final manuscript: final author's manuscript post peer review, without publisher's formatting or copy editing

Straddling the tholeiitic/calcalkaline transition: the effects of modest amounts of water on magmatic differentiation at Newberry Volcano, Oregon.

Ben E. Mandler*[1], Julie M. Donnelly-Nolan[2], Timothy L. Grove[1].

[1]Department of Earth, Atmospheric and Planetary Sciences, Massachusetts Institute of Technology, 77 Massachusetts Avenue, Cambridge MA 02139.

[2]U.S. Geological Survey, 345 Middlefield Road, Menlo Park, CA 94025.

*Corresponding author: bmandler@mit.edu, 617-253-2876.

Keywords: experimental petrology; fractional crystallization; Cascade arc; Newberry Volcano; dacite.

Abstract

Melting experiments have been performed at 1 bar (anhydrous) and 1 and 2 kbar H_2O-saturated conditions to study the effect of water on the differentiation of a basaltic andesite. The starting material was a mafic pumice from the compositionally zoned tuff deposited during the ~75 ka caldera-forming eruption of Newberry Volcano, a rear-arc volcanic center in the central Oregon Cascades. Pumices in the tuff of Newberry caldera (TNC) span a continuous silica range from 53 to 74 wt.% and feature an unusually high Na_2O content of 6.5 wt.% at 67 wt.% SiO_2. This wide range of magmatic compositions erupted in a single event makes the TNC an excellent natural laboratory in which to study the conditions of magmatic differentiation. Our experimental results

and mineral-melt hygrometers/thermometers yield similar estimates of pre-eruptive H_2O contents and temperatures of the TNC liquids. The most primitive (mafic) basaltic andesites record a pre-eruptive H_2O content of 1.5 wt.% and a liquidus temperature of 1060-1070°C at upper crustal pressure. This modest H_2O content produces a distinctive fractionation trend that is much more enriched in Na, Fe and Ti than the calcalkaline trend typical of wetter arc magmas, but slightly less enriched in Fe and Ti than the tholeiitic trend of dry magmas. Modest H_2O contents might be expected at Newberry Volcano given its location in the Cascade rear-arc, and the same fractionation trend is also observed in the rim andesites of the rear-arc Medicine Lake volcano in the southern Cascades. However, the Na-Fe-Ti enrichment characteristic of modest H_2O (1-2 wt.%) is also observed to the west of Newberry in magmas erupted from the arc axis, such as the Shevlin Park Tuff and several lava flows from the Three Sisters. This shows that modest-H_2O magmas are being generated directly beneath the arc axis as well as in the rear-arc. Because liquid lines of descent (LLDs) are particularly sensitive to water content in the range of 0-3 wt.% H_2O, they provide a quantitative and reliable tool for precisely determining pre-eruptive H_2O content using major element data from pumices or lava flows. Coupled enrichment in Na, Fe and Ti relative to the calcalkaline trend is a general feature of fractional crystallization in the presence of modest amounts of H_2O, which may be used to look for "damp" fractionation sequences elsewhere.

Introduction

The profound effect of water on the stability and composition of minerals during fractional crystallization has long been known from experimental work (Yoder and Tilley 1962; Eggler 1972). Sisson and Grove (1993) demonstrated that the influence of water changes the proportions

and compositions of crystallizing minerals, promoting the early appearance of olivine, pyroxene and Fe-bearing oxides and destabilizing plagioclase. "Wet" magmas therefore evolve by fractional crystallization to high SiO_2 and low FeO, while dry magmas initially become FeO-enriched at relatively constant SiO_2 (Grove and Baker 1984) and retain this elevated FeO content relative to wet magmas even once they achieve higher SiO_2 contents. As such, the pre-eruptive water content is one of the most important controls on a magma's compositional evolution, and the presence or absence of water underlies the first-order classification of subalkaline rocks into calcalkaline (FeO-depleted, SiO_2-enriched) and tholeiitic (FeO-enriched, lower-SiO_2) series, respectively (Sisson and Grove 1993).

Volcanic rock suites commonly preserve a range of compositions that allow the crystallization history of the magma, or liquid line of descent (LLD) to be determined. Because the LLD of a magma is so sensitive to water, the compositional variation preserved in each suite holds great potential for revealing the pre-eruptive water content of the magma. Because most magmatism on Earth tends to be either dry (0.1 to 0.3 wt.% H_2O – mid-ocean ridges and most intraplate volcanism; Johnson et al. 1994) or wet (3 to > 6 wt.% H_2O – volcanic arcs; Anderson 1979; Sisson and Layne 1993; Plank et al. 2013), these end-member scenarios have been well characterized and the distinguishing features of their LLDs are well-understood (Grove and Bryan 1983; Juster et al. 1989; Hess 1992; Sisson and Grove 1993). However, the "damp" region in between remains relatively unexplored, and cannot be easily resolved by interpolation because the effects of water are non-linear (Falloon and Danyushevsky 2000; Danyushevsky 2001; Médard and Grove 2008; Almeev et al. 2012). In this paper, we use the terms "dry" and "low-H_2O" to refer to magmas with typically <0.3 wt.% H_2O; we use "damp" and "modest H_2O" to

refer to magmas with 1-2 wt.% H_2O; and we use "wet" and "high H_2O" to refer to magmas with > 3 wt.% H_2O.

Mantle melting in subduction zones is initiated when H_2O released from the subducted oceanic lithosphere rises into the hotter, shallower overlying mantle wedge to produce H_2O-rich arc magmas by hydrous melting. Additionally, melts can be produced through dry adiabatic decompression melting associated with the vertical component of mantle flow into the wedge and/or the influence of back-arc spreading (Grove et al. 2002; Kelemen 2003; Kelley et al. 2006). The general expectation is that wet fluid-fluxed melts will dominate in the arc and that the influence of fluid-assisted mantle melting will diminish moving from the arc axis away from the trench, such that back-arc magmas will be produced largely by decompression melting (e.g. Kelley et al. 2006). However, these decompression melts are variably influenced by slab-derived fluids and may contain 0-2 wt.% H_2O (Stolper and Newman 1994; Danyushevsky 2001; Kelley et al. 2006; Langmuir et al. 2006). Furthermore, in several arc settings melts in close spatiotemporal association can be both hydrous and anhydrous (Tatsumi et al. 1983; Bartels et al. 1991; Kinzler et al. 2000; Grove et al. 2002), indicating that both hydrous and decompression (anhydrous) melting processes are operating across arcs. The production of damp melts is a likely result of the interplay of these two melting mechanisms (e.g. Langmuir et al. 2006), and could occur by mixing between dry and wet melts, or by decompression-assisted melting of the mantle wedge in the presence of small amounts of water.

Anhydrous (dry) and hydrous (wet) magmatic differentiation are now quite well-understood (see above); to fully understand the range of differentiation processes occurring at arcs, some insight into how damp magmas form and evolve is needed. In this paper, we present field and experimental evidence for the prevalence and distinguishing characteristics of damp

magmas at Newberry Volcano, Oregon. We show that these magmas are characterized by enrichment in Na, Fe and Ti relative to calc-alkaline magmas, and that this compositional signature is produced by fractional crystallization in the presence of 1-2 wt.% H_2O. Although these compositions represent a minor component of observed arc volcanism (e.g. Ewart 1979, 1982), this signature of modest magmatic water contents is observed at a number of other volcanic centers in the Cascades, including the High Cascades west of Newberry Volcano.

Geologic Setting

This study focuses on the compositionally zoned basaltic andesite to rhyolite tuff that erupted to form Newberry caldera about 75,000 years ago (Donnelly-Nolan et al. 2011). The 6 x 8 km caldera occupies the center of Newberry Volcano (Figs. 1 & 2), a broad, shield-shaped volcano whose lavas cover ~3000 km^2 in the rear-arc of the central Oregon Cascades. The main edifice rises a kilometer in prominence over its surroundings and is comprised of hundreds of discrete vents (MacLeod et al. 1995; Jensen et al. 2009; Donnelly-Nolan et al. 2011). Since the caldera-forming eruption, erosion and burial by younger lavas have resulted in limited exposures, but initially the eruption produced lobes of ash-flow and ash-fall tuff that were widely distributed around the flanks of the volcano and beyond. Sample locations where pumices were collected are shown in Fig. 2.

Petrology and geochemistry of pumices

Sparsely phyric to aphyric pumices were collected from the tuff of Newberry caldera (TNC). Some pumices with larger crystal cargoes (5-10 %) were also included in the final dataset because our new experimental phase equilibria (below), bulk compositions and mineral

compositions indicate that the crystals are equilibrium phenocrysts and do not represent crystal accumulation or xenocryst entrainment. Pumices with a true phenocryst cargo will still lie on the same LLD as the glass (groundmass) composition alone. The presence of phenocrysts will simply make the pumice plot at a slightly earlier / less evolved point on the LLD than would the glass. All of the pumices typically contain <1% of small (<5 mm) granitoid inclusions in various states of disaggregation, from well-preserved xenoliths to dispersed plagioclase xenocrysts. Most pumices also contain a true phenocryst assemblage making up <3% of the rock. These are typically found in glomerocrysts ranging from a few 10s of μm to several mm, depending on the sample (Fig. 4); in more mafic pumices, phenocrysts are sufficiently small to give an aphyric appearance to the hand sample.

In total, 97 pumices were collected. XRF analyses for major, minor and trace elements were performed at the USGS and WSU; the full dataset is available with analytical methods in the supplementary information. Pumice compositions are illustrated in Fig. 3; representative compositions are given in Table 1. The pumices record continuous compositional variation from 53 to 74 wt.% SiO_2 (Fig. 3), and their compositional trend is distinctive in having an unusually high Na_2O peak of 6.5 wt.% at 67 wt.% SiO_2, as well as elevated FeO and TiO_2 contents at a given SiO_2 content compared to calcalkaline differentiation trends. The entire suite of pumices falls in the tholeiitic field as defined by Miyashiro (1974), with most compositions plotting close to the tholeiitic-calcalkaline boundary. The TNC is unusual in that a single eruptive event deposited a wide range of magmatic compositions that record a continuous liquid line of descent (LLD). This dataset allows us to thoroughly probe the processes responsible for the observed compositional variation.

Seven pumices are excluded from Fig. 3 because they form a low-Na trend with elevated Al_2O_3 (Fig. 5) that is distinct from the rest of the data and more like a typical calcalkaline trend. These samples are mostly from a single locality, are not genetically related to the rest of the pumices, and do not represent mixing between mafic and silicic compositions (Fig. 5). They are stratigraphically low in the tephra sequence and erupted early as a discrete batch of magma, perhaps prior to the main caldera-forming eruption. The rest of the pumices form tight trends in composition space for samples with <67 wt.% SiO_2, at which point there is a notable kink in SiO_2-Na_2O. Above 67 wt.% SiO_2, the data become slightly more dispersed (Fig. 3).

Two pumices (692Ja & 272Ja; Table 1, Figs. 2 & 3) were chosen for further study and as starting materials for the experiments. 692Ja represents one of the most primitive (mafic: lowest SiO_2, highest MgO) compositions in the TNC and contains very few granitoid micro-inclusions (<< 1%), making it an excellent starting material. The sample was selected from a suite of near-identical large pumices (20-35 cm across) in the ash-flow tuff of the TNC. It is an aphyric basaltic andesite comprised of ~90 % groundmass and 10 % microphenocrysts (20-100 μm), as determined on a vesicle-free basis by relative area calculations on thick sections. The microphenocryst assemblage is strongly dominated by plagioclase (An_{50}), with lesser clinopyroxene (Mg# = 0.70), olivine (Mg# = 0.68) and Fe-Ti oxides. Larger (>400 μm) plagioclase xenocrysts make up << 1% of the sample and form a bimodal but continuous compositional distribution with modes at An_{60} and An_{22}. Glomerocrysts containing all four microphenocryst phases are common (Fig. 4a) and have identical phase compositions to the other microphenocrysts. The groundmass is dominated by <10 μm clinopyroxene and plagioclase with minor Fe-Ti oxides and interstitial glass.

272Ja is a dacite with 66.3 wt.% SiO_2 and 6.38 wt.% Na_2O, making it one of the highest-Na samples in the TNC (Table 1; Fig. 3). It was chosen as the starting material for experiments exploring further fractional crystallization of the high-Na trend beyond the peak at 67 wt.% SiO_2 and into the rhyolitic compositional range. The sample was selected from a suite of near-identical dark grey pumices 15-35 cm in diameter in another ash-flow tuff outcrop 6.5 km from the 692Ja site. Three of these pumices were chosen for detailed petrographic study. The pumices are variably streaked with dark glassy regions. Unstreaked regions are sparsely phyric with large (up to several mm) glomerocrysts consisting of equilibrium orthopyroxene (Mg# = 0.60), plagioclase (An_{31}), apatite and Fe-Ti oxides (Fig. 4b). Glomerocrysts are typically surrounded by crystal-free glass, which has a composition approximately equal to that of the bulk pumice minus the glomerocrysts, further indicating that these glomerocrysts are cognate. These pumices contain a negligible amount of xenolithic material.

The pumices' phenocrysts record the equilibrium mineral assemblage present in these liquids at magma chamber conditions. We can use this to inform our experiments, which aim to reproduce the chemical trends preserved in the pumices by crystallizing the correct minerals and mineral compositions. The presence of olivine, clinopyroxene, plagioclase and Fe-Ti oxide in 692Ja indicates sufficient H_2O to stabilize FeTi oxides early in the crystallization sequence but not enough to strongly destabilize plagioclase. The absence of amphibole as a phenocryst in the more evolved sample 272Ja further indicates that water contents were not sufficiently high to stabilize this hydrous phase. We therefore focused our experimental study on 1 kbar H_2O-saturated conditions (~3 wt.% H_2O), with two further series of experiments at 1 atmosphere (~0 wt.% H_2O) and 2 kbar H_2O-saturated (~6 wt.% H_2O) to more rigorously assess the effects of H_2O on magmatic evolution.

Experiments

Experimental Methods

Experiments were conducted at the MIT experimental petrology lab on a variety of starting materials with the bulk composition of sample 692Ja (Table 1). These different starting materials were used to assess the effects of unreacted crystal cores in natural samples and the availability of nucleation sites on the stability and composition of experimentally produced phases. Natural powders and synthetic oxide powders were both used. In the natural powder experiments, the existing minerals in the starting material acted as seeds for the new minerals grown in the experiments. In a second set of seeded experiments, the natural powder was mixed in a 9:1 ratio with a powdered mineral mixture composed of extreme mineral compositions (bytownite, microcline, magnesian orthopyroxene, quartz and end-member diopside, albite and fayalite), but with the same bulk composition as 692Ja (Table 2). These seeds were far from equilibrium with the melt and were used to test whether the composition of the seeds affected the composition of the minerals grown during experiments. Experiments conducted on sample 272Ja used only natural powders.

Experiments followed procedures described in Sisson and Grove (1993), with modifications as follows: 1 and 2 kbar H_2O-saturated experiments were conducted in molybdenum-hafnium-carbide (MHC) cold-seal pressure vessels. The oxygen fugacity (f_{O_2}) was buffered at Ni-NiO (NNO). Although the f_{O_2} conditions of the TNC have not been directly determined, the rim andesites of the rear-arc Medicine Lake volcano in the southern Cascades, which have a very similar compositional trend to the TNC, have an f_{O_2} of NNO-0.6 to NNO as

determined by two-FeTi-oxide oxybarometry (J. Fuentes, unpublished data). This suggests that the NNO buffer is appropriate for experiments on the TNC. The f_{O_2} was maintained at the NNO buffer by packing Ni and NiO in a 4:1 mass ratio into Pt capsules, which were incompletely welded to leave a small hole in the top. Sample powders were packed into Au capsules with powder/capsule weight ratios > 0.2 to minimize Fe loss (Ratajeski and Sisson 1999). These capsules were similarly welded and placed together with the buffer capsules into a larger Au outer capsule, to which 13-25 µl of doubly deionized water was added before the outer capsule was fully welded. During the experiments, the small holes in the inner capsules allowed supercritical H_2O to effectively transport oxygen between the inner capsules while otherwise chemically isolating the Ni-NiO mixture from the sample.

The pressure vessel was charged with argon and methane in a 2000:21 (1 kbar) or 2000:34 (2 kbar) ratio to minimize hydrogen loss from the sample. After pressurization, the vessel was placed in a Deltech DT31VT furnace and brought up to the run temperature over the course of an hour, while excess pressure was bled out of the system. The vessel was then held at constant pressure and temperature for the duration of the experiment. Experiments were quenched by removing the pressure vessel from the furnace, inverting it and striking the hot end of the pressure vessel with a wrench. The capsule dropped to the water-cooled end of the pressure vessel and quenched rapidly with no growth of quench crystals. The capsule was then checked for the presence of water, Ni and NiO to confirm that water-saturated, f_{O_2}-buffered conditions prevailed for the duration of the experiment. Samples were then mounted and polished for electron microprobe analysis.

One-bar experiments were conducted to determine the 1-bar liquidus and the nominally anhydrous liquid line of descent for composition 692Ja. Sample powders were blended with

elvanol and dried onto PtFe-alloy loops. These loops were suspended from a Pt wire in a Deltech DT31VT furnace, at which point the elvanol burned off and the partially molten sample remained on the loop due to surface tension. Oxygen fugacity was maintained at the NNO buffer using a mixture of CO_2 and H_2 gases. Experiments were quenched by running a current through the Pt wire, which melted the wire and dropped the loop into a bowl of water beneath the furnace, quenching the sample. Compositions of phases in the experimental starting material and experimental products were obtained using a five-spectrometer JEOL JXA-8200 Superprobe at the electron microprobe facility at MIT.

Experimental Results

Experimental conditions and phase assemblages are given in Table 3. Chemical analyses of experimental run products are given in Table 4; experimental glass analyses are plotted along with TNC pumice compositions in Fig. 6. Phase proportions were estimated by mass balance using traditional least squares techniques (Bryan et al. 1969). In runs 692Ja-1 & 2 and 272Ja-1 & 2b, high-Ca pyroxenes (692Ja experiments) or Ti-rich oxides (272Ja experiments) were not large enough to obtain reliable analyses, hence their absence from Table 4. For these experiments, estimated phase compositions were used to calculate phase proportions. These estimates were based on compositions of the same phases in other experiments at similar conditions. All reasonable estimates gave the same phase proportions to within 1 wt. %.

Experimental equilibrium and applicability to the natural system

Iron loss was tested in several ways: (1) Glass analyses showed that one super-liquidus experiment (692Ja-23) reproduced the bulk composition of the starting material, including FeO

content, to within analytical uncertainty (Table 4); (2) In all high-pressure runs, analyses of glass within 100 µm of the wall of the Au sample capsule showed that Fe loss was negligible except in run 45, which experienced minor Fe-loss only at the very edge of the charge; (3) Fe loss was estimated using mass balance calculations and found to be <0.2 % in all experiments except two 1 bar experiments (692Ja-4 & 6), which gained a small amount of Fe from the PtFe loop (Table 3).

Experiments on synthetic oxide powders rarely grew crystals large enough for reliable analysis, particularly in lower-temperature runs. In experiments on natural samples, relict cores of pre-existing crystals (original minerals in the sample and/or added seed crystals) were surrounded by experimentally grown rims. Mineral analyses given in Table 4 were taken only on crystal rims in contact with melt. For each rim analysis, the core was also analyzed. Crystal rim compositions were constant throughout each sample capsule. Furthermore, for experiments conducted at the same P-T-H_2O conditions but using either the natural powder or a mixture of the natural powder and seed crystals very far from equilibrium with the melt, the compositions of mineral rims were identical. This indicates that the presence and composition of mineral cores have a negligible effect on the experimental phase equilibria. Having established this, the majority of the experiments reported in this paper were performed using only the natural powder as the starting material. The consistency of rim compositions and exchange coefficients (K_Ds; Table 3), textural equilibrium between rim and melt, and absence of any correlation between core and rim compositions suggest a close approach to rim-melt equilibrium.

The three experimental series conducted here reproduce equilibrium crystallization paths, rather than the near-fractional or incremental equilibrium crystallization that occurs in many magma chambers (e.g. Allègre et al. 1977). However, liquid evolution during equilibrium

crystallization is very similar to fractional crystallization as long as the melt fraction remains high (>30 %) and as long as no reaction boundaries or peritectics are encountered. For the 1 kbar experiments in this study, we take advantage of this by conducting experiments such that the lowest-temperature run using sample 692Ja and the highest temperature run using sample 272Ja are on either side of the peritectic marked by the transition from olivine to low-Ca pyroxene crystallization (run 692Ja-45 contains olivine but no orthopyroxene, while run 272Ja-1 contains orthopyroxene but no olivine). Sample 272Ja represents a more evolved composition on the same liquid line of descent as sample 692Ja; by using it as the starting composition for the lowest-temperature 1 kbar runs, we both bypass the peritectic and maintain a high melt fraction. We can therefore confidently use these experiments to explore fractional crystallization of the TNC magma.

H_2O contents, phase stability and liquid lines of descent

Fig. 7 shows the appearance temperatures of mineral phases in this study. This represents the H_2O-saturated phase diagram for composition 692Ja. Although we have not directly measured the H_2O content of our experimental glasses, many studies have experimentally calibrated the effect of pressure on the solubility of H_2O in melts (e.g. Dixon et al. 1995; Moore et al. 1998; Lesne et al. 2011). We take advantage of the fact that our 1 and 2 kbar experiments were H_2O-saturated to use these calibrations to estimate H_2O contents in our melts. The 1 kbar experiments had H_2O contents of 3 – 3.5 wt.%, while the 2 kbar experiments had H_2O contents of ~6 wt.%. These values also approximately match the sum deficits obtained in our microprobe analyses of the experimental glasses (Table 4). Based on the calibrations referenced above and considering the small compositional dependence of H_2O solubility, we estimate uncertainties of ±0.5 wt.%

H_2O for these figures. With these uncertainties in mind, we refer to the 1 kbar experimental liquids as containing 3 wt.% H_2O and the 2 kbar liquids as containing 6 wt.% H_2O.

At 1 atmosphere (0 wt.% H_2O), the liquidus is at ~1160°C and the down-temperature order of mineral saturation is: plagioclase → olivine → clinopyroxene + FeTi-oxide + pigeonite (and disappearance of olivine) → apatite. The differences in the down-temperature evolution of the melt at each pressure are largely caused by higher P_{H_2O} progressively destabilizing plagioclase relative to other silicates and particularly FeTi oxides, and ultimately stabilizing amphibole at higher P_{H_2O}.

At 1 kbar (3 wt.% H_2O), the liquidus is lowered by ~130°C, with clinopyroxene and FeTi-oxide as the stable liquidus phases at ~1030°C. Plagioclase, olivine and apatite all join the crystallizing assemblage between 985°C and 970°C, while the replacement of olivine by orthopyroxene occurs at ~ 930°C.

At 2 kbar (6 wt.% H_2O), the liquidus has been depressed a further ~45°C. Clinopyroxene and FeTi-oxide remain the liquidus phases, at ~985°C, with amphibole crystallizing below ~ 960°C. Olivine is completely destabilized in the 2 kbar experiments, while apatite and plagioclase are not observed, though they probably crystallize at temperatures below the lowest-temperature 2 kbar experiments in this study (950°C).

These differences in crystallization sequence can be clearly identified in the element variation diagrams of Fig. 6: early plagioclase crystallization and relatively late FeTi oxide crystallization make dry melts evolve to lower Al and higher Fe & Ti, while in wet melts, plagioclase suppression and FeTi oxide crystallization enrich the melt in Al and deplete it in Fe & Ti.

Discussion

Generating high-Na dacites: pre-eruptive magmatic conditions

Fig. 6 shows that the 1 kbar experiments reproduce the liquid line of descent (LLD) of the TNC liquids much more successfully than 2-kbar or 1-bar experiments. The effect of pressure itself is very small over this interval; instead, the differences between the three experimental series are due to differences in melt H_2O content: ~0%, 3% and 6% at H_2O saturation for 1 bar, 1 kbar and 2 kbar, respectively. The more water in the melt, the later plagioclase crystallizes and the earlier FeTi oxides crystallize (Fig. 7), so wetter melts evolve to higher Al_2O_3 and lower FeO and TiO_2. Although the 1 kbar (3 wt.% H_2O) experiments are the closest fit of the three series, they still contain too much water, as evidenced by enrichment in Al_2O_3 and slight depletion in FeO and TiO_2 relative to the TNC pumices (Fig. 6). So the water content of the TNC magma was less than 3%, but how much less?

The experimental phase equilibria can help here. Remembering that sample 692Ja is multiply saturated in plagioclase, olivine, clinopyroxene and an FeTi oxide (Fig. 4a), an experiment reproducing the true magmatic storage conditions of this sample should be multiply saturated in all four of these phases at the liquidus. Interpolation of phase stabilities from the three experimental series shows that this occurs at ~1.5 wt.% H_2O (Fig. 7). Uncertainties from H_2O solubility and interpolation of phase boundaries are estimated at ±0.5 wt.% H_2O.

This interpretation is fully consistent with all minor deviations of the 1 kbar experimental liquids from the TNC liquids in terms of other elements, notably K_2O, FeO and TiO_2. Figure 8 shows how these deviations arise. Lower H_2O yields a crystal assemblage with more plagioclase and less FeTi oxide, which is therefore higher in SiO_2. The bulk crystal assemblage still has very

low K_2O, but its higher SiO_2 content drives up K_2O in the melt more rapidly relative to SiO_2. The bulk crystal assemblage in a water-poor system would also have lower FeO and TiO_2 due to the lower proportion of FeTi oxides, which would result in less depletion of FeO and TiO_2 in the melt than in the 1 kbar experiments. Other elements would not be strongly affected. For example, CaO is quite insensitive to H_2O content: higher H_2O suppresses plagioclase crystallization but stabilizes a Ca-bearing amphibole, thereby removing similar amounts of CaO from the melt. MgO is similarly insensitive to melt H_2O content.

The change in Na_2O with increasing SiO_2 is particularly sensitive to H_2O (Fig. 8). In very dry melts, plagioclase is both abundant and Na-rich, leading to Na-depletion in the melt. However, at high water contents (~6 wt.% H_2O), Na-bearing amphibole is stable, producing a low-SiO_2 but moderate-Na crystal assemblage that only leads to mild Na-enrichment. To achieve the Na enrichment seen in the TNC, intermediate H_2O contents are required to partly destabilize plagioclase and make the plagioclase more Ca-rich without stabilizing amphibole; to satisfy this and all other compositional features of the TNC LLD requires 1-2 wt.% H_2O.

To further constrain the water content of the TNC liquids, we can apply existing hygrometers and thermometers to the pumices and their equilibrium phenocryst assemblages. The best-calibrated hygrometer for this system is the exchange of Ca and Na between plagioclase and liquid. This has long been known to be strongly dependent on melt H_2O content (Sisson and Grove 1993), and was more recently calibrated by Lange et al. (2009), who incorporated the effects of temperature and pressure to produce an improved hygrometer.

To apply the Lange et al. (2009) hygrometer to TNC pumices, the temperature and pressure must be known. Using our experimental phase equilibria (Fig. 7) and a range of mineral-melt thermometers (see below and Table 5), we estimate the original magmatic

temperature of sample 692Ja to be 1060-1070°C. We estimate the pressure to be 1 kbar, assuming shallow H_2O-undersaturated conditions (see section "Effect of pressure", below), and we note that the pressure sensitivity of this calculation is very small (<0.1 wt.% H_2O / kbar). Using these parameters and the plagioclase composition from equilibrium phenocrysts, we obtain a magmatic H_2O content for 692Ja of 1.4 wt.%. Sample 272Ja represents a liquid derived by ~50% fractional crystallization of sample 692Ja, as determined from our 1 kbar experiments and simple modeling (Table 3, and section "Modeling TNC liquid evolution using phenocryst compositions", below). For this sample, we use an estimated liquidus temperature of 970°C and a pressure of 1 kbar. Based on the average plagioclase composition of three near-identical pumices from the 272Ja site, we obtain a magmatic H_2O content for 272Ja of 2.8 wt.%. This suggests that the TNC liquids were H_2O-undersaturated and became progressively enriched in H_2O as crystallization progressed. However, we suggest this with some caution because the composition of the plagioclase in the pumices from site 272Ja (An_{31}) is slightly outside the range for which the Lange et al. (2009) hygrometer is calibrated (An_{37}-An_{93}).

A second way that we have estimated both the magmatic H_2O content and temperature of sample 692Ja is to use a range of empirical mineral-melt and melt-only thermometers that have an H_2O-dependence (mineral-melt) and two that do not (melt-only; Putirka 2008). Varying the H_2O input in the mineral-melt thermometers causes the temperature estimates to vary significantly, while the melt-only thermometers are insensitive to H_2O content. If temperatures are calculated for a range of H_2O contents, the two groups of thermometers should give the same answer at the true H_2O content and systematically diverge in their predictions for H_2O contents that are too high or low. Table 5 shows the range of predicted temperatures for 0-3 wt.% H_2O at 1 kbar. Although there is a modest range in temperature predictions among the different

thermometer-hygrometers (Table 5), the averages of the two groups converge at 1069°C and 1.4 wt.% H_2O.

A third method for estimating H_2O content, also involving plagioclase but independently calibrated, is the peak Al_2O_3 content in a liquid line of descent (Parman et al. 2011). This is controlled by the appearance of plagioclase on the liquidus (at which point Al_2O_3 decreases) and so is a good indicator of the H_2O content of the melt. The experimentally calibrated relationship between melt H_2O content at plagioclase appearance and the associated melt Al_2O_3 content is defined by Parman et al. (2011) as: $H_2O_{plag\text{-}in} = 1.34\ Al_2O_3^{max} - 21.05$. The TNC pumices studied here do not extend back to primitive basaltic compositions and are all plagioclase saturated. However, a suite of Fe-Ti-rich basalts and basaltic andesites that erupted from Newberry just prior to the caldera-forming eruption overlaps the TNC pumices in composition space. These basalts appear to be more primitive members of the same LLD (Fig. 3), extending back to 52 wt.% SiO_2 and 4.7 wt.% MgO (Table 1). They do not exceed 16.5 wt.% Al_2O_3, indicating that Al_2O_3 concentrations in this LLD remain nearly constant at 16-16.5 wt.% from 52 wt.% SiO_2 and 4.7 wt.% MgO to 63 wt.% SiO_2 and 1.8 wt.% MgO (Fig. 3). Extrapolating this trend back to plagioclase saturation yields a maximum Al_2O_3 content of 16.5 wt.% unless plagioclase crystallizes significantly earlier than FeTi oxides. Given that the most mafic pre-caldera basalts are saturated in both FeTi-oxide and plagioclase, any realistic scenario yields a maximum Al_2O_3 content of 16.5-17 wt.%. Using the Parman et al. (2011) Al_2O_3 hygrometer, this corresponds to an H_2O content of 1.1-1.7 wt.%. However, the scatter in the calibration for this hygrometer is particularly large at low H_2O contents. This hygrometer therefore indicates only that the H_2O content in the mafic TNC magmas was <2 wt.%.

Effect of pressure

The pressure at which the TNC magmas differentiated is hard to constrain. As mentioned above, the effect of pressure on phase equilibria at upper crustal conditions is very small. However, higher pressures typical of the lower arc crust have a significant effect on phase stability. It is therefore worth considering whether high-pressure differentiation could have produced the compositional trends of the TNC pumices.

High-pressure *anhydrous* differentiation (7 & 10 kbar) has been explored by Villiger et al. (2004; 2007). Their experimental melts deviate from the TNC in many ways, but one of the most significant effects is that the destabilization of FeTi oxides by elevated pressure (in addition to the absence of H_2O) caused the melt to evolve to TiO_2 contents and FeO/MgO ratios considerably greater than those of the TNC.

High-pressure *hydrous* differentiation (3-10 wt.% H_2O, 7 kbar) has been recently explored by Nandedkar et al. (2014). Plagioclase is strongly destabilized by both high pressure and high H_2O, so Al_2O_3 contents in their experimental LLD exceeded 20 wt.% for basaltic andesite compositions, compared to a maximum of 16.5 wt.% in the TNC. Furthermore, the stabilizing effect of high H_2O on FeTi oxides counters the destabilizing effect of pressure, such that the LLD did not exceed 1 wt.% TiO_2 and remained firmly in the calcalkaline field (c.f. >2 wt.% TiO_2 and mildly tholeiitic character for the TNC).

High-pressure differentiation of magmas with more moderate H_2O contents has been studied by Blatter et al. (2013), who performed experiments on fractionation trends at 4, 7 and 9 kbar for a fixed bulk H_2O content of 2 wt.%. Higher pressures and moderate H_2O contents suppress both plagioclase and FeTi oxide crystallization, so high-Na_2O mafic magmas (4.5 wt.% Na_2O at 55 wt.% SiO_2) with somewhat elevated FeTi can be produced by fractional

crystallization at high pressures (7-9 kbar; Blatter et al. 2013). However, because plagioclase is so strongly suppressed at these pressures, these melts also evolved to extremely high Al_2O_3 contents of ~20 wt.% in the 7 and 9 kbar experiments. Furthermore, although high-Na_2O *mafic* magmas can be produced by high-pressure fractionation, very high-Na_2O *dacites* cannot. Na_2O contents in the experiments of Blatter and coworkers did not exceed 4.8 wt.% and declined with continued fractionation to higher silica contents (3.5 – 4.0 wt.% Na_2O at 62 wt.% SiO_2 in the 7 and 9 kbar experiments) due to crystallization of large quantities of Na-bearing amphibole and plagioclase. The existing experimental literature on lower crustal differentiation therefore supports an upper crustal environment for differentiation of the TNC liquids.

Fractional vs. Equilibrium Crystallization

The relative roles of fractional and equilibrium crystallization can be investigated using Rb and Ba concentrations in the TNC pumices. For plagioclase-dominated systems such as this one, Rb is highly incompatible until very evolved compositions, while Ba changes from being slightly incompatible to increasingly compatible in plagioclase as it becomes more albitic (e.g. Blundy and Wood 1991). Therefore, melts undergoing equilibrium crystallization will become progressively enriched in Rb, but will be first enriched and then depleted in Ba as it is preferentially repartitioned into increasingly albitic plagioclase. Conversely, melts undergoing fractional crystallization are strongly enriched in both Rb and Ba until at least 85 % crystallization. Using estimated temperatures, phase proportions and compositions determined from our experiments and the mineralogy of the TNC pumices, we have modeled Rb and Ba behavior for equilibrium and fractional crystallization of sample 692Ja (Fig. 9; Table 6). We use

the empirical expression of Blundy and Wood (1991) for plagioclase-liquid Ba partitioning as a function of plagioclase composition:

$$RTlnD_{Ba}^{plag-liq} = 10200 - 38200X_{An}$$

where R is the gas constant, T is temperature in K, D is the partition coefficient of Ba between plagioclase and the liquid, and X_{An} is the mole percent of the anorthite component in plagioclase. Additional partition coefficients for the other phases come from Rollinson (1993) and the GERM database (Table 6). The system is so strongly dominated by plagioclase that uncertainties in the small values of partition coefficients for other phases have a negligible effect on the results.

Rb-Ba systematics of the TNC pumices in the 53-67% SiO_2 range show that fractional crystallization dominated over equilibrium crystallization in the Newberry system. The ability of fractional crystallization to explain not only major element variation (from our experiments) but also trace element data lends credence to our assertion that fractional crystallization was the dominant process that produced the compositional variability in the TNC. The Rb-Ba data also suggest that the rhyolitic pumices, though more variable in composition, could have been derived from the high-Na-trend liquids by fractional crystallization.

Are the high-Na trend and the rhyolites genetically related?

Two experiments were performed on the high-Na dacite sample 272Ja to investigate the effects of continued fractionation into the rhyolite compositional range. The experimentally produced liquids in the 272Ja runs show that continued fractionation past 67 wt.% SiO_2 depleted the high-Na liquids in Na_2O, reproducing the kink in the Na_2O-SiO_2 systematics of the TNC pumices (Figure 6). This can be explained by the changes in mineral stability observed in these experiments and in the pumices from the 272Ja site. The experiments on samples 692Ja and

272Ja indicate that the olivine-out/orthopyroxene-in reaction occurs near 67 wt.% SiO_2 (run 692Ja-45 at 935 °C contains olivine but no orthopyroxene, while run 272Ja-1 at 920 °C contains orthopyroxene but no olivine). This is supported by the absence of olivine and presence of orthopyroxene phenocrysts in the 272Ja pumices. Additionally, the 272Ja pumices lack clinopyroxene, and the 272Ja experiments contained only small, rare clinopyroxenes.

The kink in the Na_2O-SiO_2 systematics of the TNC pumices can therefore be explained as follows: when the liquid had evolved to ~67 wt.% SiO_2, it reached the olivine-orthopyroxene peritectic. In addition to the olivine-out / orthopyroxene-in reaction, the proportion of clinopyroxene in the crystallizing assemblage significantly decreased, and the proportion of plagioclase in the crystallizing assemblage significantly increased. The bulk crystal assemblage therefore became significantly more Na_2O-rich, containing a higher Na_2O concentration than the melt. The replacement of olivine by orthopyroxene and the increase in the proportion of plagioclase also increased the SiO_2 content of the bulk crystal assemblage. Fractional crystallization of this assemblage therefore depleted the melt in Na_2O for only modest increases in SiO_2. Similar kinks in SiO_2-Na_2O systematics have also been experimentally observed by Grove et al. (1997).

Liquids in our 1 kbar experiments on composition 272Ja still had higher H_2O than the TNC liquids, as indicated by slightly elevated Al_2O_3 contents (Fig. 6). With less H_2O, plagioclase would be more abundant and more albitic, leading to even more Na-depletion in the melt. These results, combined with the Rb-Ba modeling described above, indicate that rhyolites like those in the TNC can be produced by continued fractionation of the high-Na dacites.

Role of mixing and assimilation

There are several lines of evidence that show that magma mixing and assimilation did not play a significant role in producing the compositional diversity of the TNC:

1. The strong kink in the Na_2O-SiO_2 trend at 67 wt.% SiO_2 (Figs. 4 & 5) shows that mixing between basaltic-andesitic and rhyolitic compositions did not produce the intermediate magma compositions. This rules out two-component mixing.

2. If three-component mixing occurred between basaltic-andesitic, dacitic, and rhyolitic compositions, this would require that the most mafic and most silicic compositions did not mix with each other, and that each only mixed with the high-Na dacitic composition. In addition to the physical improbability of this scenario, there is strong compositional evidence against mixing between the high-Na dacitic and basaltic-andesitic compositions. Figure 3 shows the P_2O_5-SiO_2 compositions of the TNC pumices. There is a clear trend of increasing P_2O_5 with increasing SiO_2 up to 61% SiO_2, 0.75 wt.% P_2O_5, after which P_2O_5 decreases substantially with increasing SiO_2. This cannot be produced by mixing between the basaltic-andesitic magma (55% SiO_2, 0.5 wt.% P_2O_5) and the high-Na dacitic magma (67 wt.% SiO_2, 0.3 wt.% P_2O_5). However, this trend *is* consistent with a fractional crystallization origin: the melt became progressively enriched in P_2O_5 until the point of apatite saturation, at which point P_2O_5 concentrations dropped rapidly with continued fractionation. Our 1 kbar experiments indicate that apatite saturation occurs between 58 and 63 wt.% SiO_2, consistent with the 61 wt.% SiO_2 indicated by the TNC pumice data.

3. The bimodality of plagioclase xenocryst compositions in sample 692Ja may be interpreted as evidence of mixing. However, sample 692Ja contains <<1 % xenocrysts by volume, and the modes are at An_{60} and An_{22}. The plagioclase phenocrysts in pumices from the 272Ja site (67 wt.% SiO_2) are An_{31}, so the An_{22} xenocrysts in the basaltic-andesitic 692Ja must have come from more evolved rhyolitic magmas. Yet we have shown (Argument 1) that mixing

between the basaltic-andesitic and rhyolitic magmas cannot have been a significant source of compositional variability in the TNC. Instead, these xenocrysts, along with a minor (<1 %) fraction of xenoliths, represent small degrees of assimilation of wall-rock material and xenocrysts, perhaps from earlier fractionation. These assimilants may have produced some of the dispersion in the data, particularly in the rhyolitic compositions, but did not produce the general compositional trends of the TNC pumices.

Modeling TNC liquid evolution using phenocryst compositions

The petrology of the pumices and the results of our experiments suggest that the crystallizing phase assemblage did not change significantly as the liquid evolved from the more primitive compositions (e.g. 692Ja – Table 1) to the high-Na dacitic liquids (e.g. 272Ja – Table 1). In both sample 692Ja and our 1 kbar experiments, this assemblage is olivine + clinopyroxene + plagioclase + 2 FeTi oxides. The only changes that occur are: 1) the phase compositions will change slightly as the liquid evolves, and 2) apatite begins crystallizing at ~61 wt.% SiO_2 (the position of the P_2O_5 peak in Fig. 3). Inspection of Fig. 3 shows that the compositional evolution of these melts is approximately linear in all major elements from 55.9 wt.% SiO_2 to 67 wt.% SiO_2. This further shows that the crystallizing phase assemblage is of approximately constant composition until the liquid reaches 67 wt.% SiO_2. Given the compositions of phenocryst phases in 692Ja, we can model what the crystallizing phase proportions must be for the residual liquid to follow the TNC LLD up to 67 wt.% SiO_2 (we do not attempt this beyond 67 wt.% SiO_2 due to insufficient constraints on the crystallizing mineral assemblage). The problem is of the form:

$$Ep = a + tb$$

Where *E* is a matrix of phase compositions, *p* is a vector of crystal proportions, *a* is the composition of the starting liquid, *t* is a factor for the magnitude of the melt evolution vector, and *b* is the composition of the target liquid. *E*, *a* and *b* are known inputs. The model then re-arranges the problem to solve for *a* by testing 10,000 random guesses for *p* at 100 random values for *t* (within a small range defined by initial trial-and-error runs) and calculating the misfit in terms of how well the original composition is reproduced. In short, this model uses known phenocryst compositions and subtracts them from the melt in various proportions to determine which phase proportions best reproduce the liquid line of descent.

A summary of the inputs and results for this model is given in Table 7. The compositional trend from the basaltic andesites to the high-Na dacites can be reasonably reproduced by crystallizing phenocryst compositions observed in sample 692Ja in the right proportions. The small discrepancies between the model-reproduced starting liquid and the true composition of 692Ja can be ascribed to analytical uncertainty and changes in phase composition during liquid evolution. To avoid any effects of apatite crystallization from ~61 wt.% SiO_2, the target composition was chosen as sample 271Jc (Table 1), which, at 60.5 wt.% SiO_2 is at or just before apatite saturation. However, we note that the appearance of ~1 wt.% apatite in the crystallizing assemblage will not significantly affect major elements, so the results of this model represent the crystallizing assemblage (plus apatite after 61 wt.% SiO_2) up to the high-Na peak at 67 wt.% SiO_2.

The model involved random sampling of a finite number of potential phase proportions from a continuum of possibilities, so running the model multiple times produced slightly different “best” fits. The model was therefore run 50 times to assess the effects of this on the results. All 50 runs gave very similar results: the full range of best-fit crystal proportions for all

50 runs was: 53-56 wt.% plagioclase, 26-30 wt.% clinopyroxene, 2-5 wt.% olivine and 15-16 wt.% FeTi oxides. These proportions are comparable to our 1 kbar experiments, which are slightly poorer in plagioclase (because they are more H_2O-rich than the TNC liquids) but otherwise similar (Table 3). This further confirms that our experiments closely approximated the magmatic conditions that prevailed in the Newberry system prior to the eruption of the TNC.

Implications for magmatic differentiation in the presence of modest amounts of water

The compositional variability of the TNC pumices in terms of all major and minor elements fits very well with our current understanding of how water affects mineral stability (e.g. Sisson and Grove 1993). With H_2O contents intermediate between dry tholeiitic and wet calcalkaline magmas, these compositions lie close to the tholeiitic-calcalkaline transition as defined by Miyashiro (1974) (Fig. 10c). The tholeiitic-calcalkaline divide is not a real boundary or divide. Rather, it represents a transitional regime between the dry melts (0.1 to 0.3 wt.% H_2O) that dominate mid-ocean ridge and intraplate magmatism and the wet melts (3 to > 6 wt.% H_2O) that dominate volcanic arcs above subduction zones.

This study has also highlighted another feature of damp melts: evolution to unusually high Na_2O. Wet melts evolve to high SiO_2 very rapidly due to plagioclase suppression and so only experience slight Na_2O-enrichment at a given SiO_2 content. Dry melts crystallize abundant plagioclase early in their fractionation sequence, which removes Na from the melt, yielding residual melts with constant or slightly enriched Na_2O (Carmichael 1964; Juster et al. 1989). However, a modest amount of water can produce extreme Na_2O-enrichment in evolving basaltic melts by affecting plagioclase stability and composition just enough to delay SiO_2-enrichment while promoting Na_2O-enrichment of the evolving melt, as follows:

The modest amount of H_2O in the damp melt will delay plagioclase crystallization and decrease the Na_2O content of the plagioclase that eventually crystallizes (Sisson and Grove 1993). These effects promote Na_2O-enrichment in the melt. However, plagioclase is still quite stable in damp melts compared to wet melts, such that the bulk crystal assemblage in the basaltic compositional range is quite SiO_2-rich. Additionally, early in the fractionation sequence, FeTi-oxides will not yet be stable, and the high relative abundance of plagioclase compared to olivine and clinopyroxene (which has a percent-level TiO_2 content) yields a bulk crystal assemblage that also has low FeO and TiO_2. Fractional crystallization of this assemblage therefore strongly enriches the melt in Na_2O, FeO and TiO_2 for only a slight increase in SiO_2. These Na-Fe-Ti-enriched, low-SiO_2 melts are represented by the pre-caldera basalts and basaltic andesites at Newberry Volcano (Table 1; Fig. 3). When FeTi-oxides join the crystal assemblage, the residual melts more rapidly evolve to higher-SiO_2 compositions, as represented by the LLD of the TNC (Fig. 3). The modest (and increasing) water content of the melt keeps the plagioclase composition sufficiently calcic to produce continued Na-enrichment, leading to the production of high-Na dacites. FeTi-oxide crystallization decreases the FeO and TiO_2 contents of the melt, but the melts remain resolvably FeTi-rich compared to wet (calcalkaline) magmas until they reach ~68 wt.% SiO_2 (Fig. 10). Figure 8 shows in more detail how the damp melts of the TNC evolved to high-Na dacites while retaining their elevated FeO and TiO_2 concentrations relative to wet melts. The wet experimental series, with 3 & 6 wt.% H_2O (light and dark blue, respectively), crystallized too high a proportion of FeTi oxides in the andesitic compositional range, so the residual melts evolved to lower FeO and particularly TiO_2 contents.

Near-identical compositions with the same characteristic Na-Fe-Ti-enrichment and near-constant Al_2O_3 are observed in both the rear-arc and the main arc axis of the Cascades. The

andesites that form the caldera rim of the rear-arc Medicine Lake volcano (Fig. 10) (Donnelly-Nolan et al. 2008; Donnelly-Nolan 2010) display a high-Na-Fe-Ti trend; experiments run on these compositions (not reported here) under identical conditions to the TNC experiments yielded near-identical results in terms of mineral stability and melt compositions. The Shevlin Park Tuff (Conrey et al. 2002) and some dacites from the Three Sisters (Hildreth et al. 2012), which all erupted from the arc axis west of Newberry Volcano (Fig. 1), also exhibit nearly identical Na-Fe-Ti enrichment (Fig. 10). This indicates that modest-H_2O "damp" magmas are not restricted to the rear-arc; in the central Oregon Cascades, damp magmas are just as abundant (if not more so) on the arc axis.

Fig. 10 illustrates the compositional differences between volcanic centers in the southern and central Cascades. In the southern Cascades, the Lassen Volcanic Center and Mt. Shasta both exhibit very low FeO/MgO, FeO and TiO_2, and moderate Na_2O contents. Much of this can be explained by H_2O-rich differentiation, with suppression of plagioclase crystallization relative to mafic silicates and then oxides, leading to rapid SiO_2-enrichment with FeTi depletion. The presence of abundant H_2O-rich melts (commonly 6 wt.% and up to 15 wt.% H_2O) is well-documented at Mt. Shasta (Grove et al. 2005; Krawczynski et al. 2012, and references therein). This is in stark contrast to the TNC, Shevlin Park Tuff and many lavas from the Three Sisters, which show Na-Fe-Ti enrichment characteristic of modest H_2O contents (1-2 wt.%). These central Oregon volcanics are compositionally very different from Shasta and Lassen, suggesting very different processes occurring in the central and southern Cascades. A possible explanation for this could be that fluid-fluxing of the mantle plays a more dominant role in mantle melting in the southern Cascades (see discussion in Schmidt et al. 2008). In central Oregon, asthenospheric upwelling may be relatively more significant, leading to drier magmas entering the arc crust.

Medicine Lake volcano, in the rear-arc of the southern Cascades, is clearly Na-Fe-Ti-enriched relative to Lassen and Shasta (Fig. 10), but less so than most of the central Oregon segment, including Newberry Volcano, which is located a similar distance east of the arc axis (Fig. 1). These distinctions make it tempting to draw conclusions about tectonic controls on the magmatic H_2O flux to the arc crust. However, a full discussion of the tectonic settings of these volcanoes is beyond the scope of this paper. Instead, we stress two important large-scale observations: (1) Volcanoes at the arc axis and in the rear arc both produce magmas with a wide range of H_2O contents. There is no clear distinction between wet magmas on the arc axis and dry magmas behind the arc. Instead, the relative importance of fluid-assisted (wet) and decompression (dry) melting varies both spatially and temporally throughout both settings (Kinzler et al. 2000; Grove et al. 2002). This is observed in both primitive basalts (e.g. Conrey et al. 2002; Donnelly-Nolan et al. 2008; Schmidt et al. 2008; Till et al. 2013) and more evolved compositions (Fig. 10 – note that the 'Three Sisters' and 'Other Medicine Lake' fields have both FeTi-enriched (drier) and FeTi-depleted (wetter) compositions). (2) Despite this complexity, when the datasets from these volcanic centers are compared (Fig. 10), a distinction can be made between the more important role of wet magmas in the southern Cascades and damp magmas in the central Oregon Cascades.

We have chosen to focus on the central and southern Cascades because of the availability of large published datasets and our own familiarity with the region. However, a survey of GEOROC data from the northern Oregon and Washington Cascades suggests that magmas with Na-Fe-Ti enrichment are either less abundant or lack published analyses in these regions. Potential candidates for damp fractionation in the more northerly Cascades are moderately Na-

Fe-Ti enriched dacites at Mt. Jefferson (Conrey et al. 2001) and andesites-dacites at Mt. Adams (Jicha et al. 2009).

Although this paper has focused on the Cascades, similar Na-Fe-Ti enrichment trends are observed elsewhere. Shishaldin in the Aleutians shows very similar Fe-Ti systematics to the TNC (Zimmer et al. 2010, and references therein), and though there are very few samples in the andesite-dacite range, most of these are moderately Na-enriched. Melt inclusion data from Shishaldin yield an H_2O content for these magmas of 2 wt.% (Zimmer et al., 2010), very similar to our estimate for the TNC. Two other notable examples are Aniakchak, also in the Aleutians (George et al. 2004), and lavas from the Witu Islands, particularly Garove island (Johnson et al. 1978), which lies 120 km behind the New Britain arc.

Na-enrichment is a common but not ubiquitous feature of damp, FeTi-enriched magmas. This may reflect a requirement for sufficient Na in primary mantle melts to allow extreme Na-enrichment to occur, although the absence of more primitive members of the TNC LLD makes it difficult to determine the initial Na_2O content of the primary mantle melt parental to the TNC liquids. Simple calculations suggest that primary mantle melts with ~3 wt.% Na_2O contain sufficient Na_2O to achieve high-Na dacitic compositions by damp fractionation. Damp melts with very low initial Na contents may evolve to FeTi-enriched compositions without the high-Na signature. If initial variations in the Na content of primary mantle melts are significant, they may reflect either the degree of mantle melting or the fertility of the sub-arc mantle. Therefore, elevated Na contents alone should not be taken as evidence for damp fractionation, nor does the absence of elevated Na contents rule out damp fractionation. Rather, it is the combination of FeTi-enrichment with Na-enrichment (or without it, depending on the initial Na_2O content) that together indicate damp (1-2 wt.% H_2O) fractionation.

Furthermore, combining Na-Fe-Ti enrichment with moderate Al_2O_3 contents (16 wt.% in the basalt-dacite range) indicates damp fractionation in the *shallow* crust. Damp fractional crystallization occurring in the deeper crust (5-10 kbar) will have a different signature. This is largely because the pressure-induced suppression of plagioclase crystallization will lead to substantial Al_2O_3 enrichment in the residual melt. It has been suggested (T. Sisson, personal communication) that the 7 & 9 kbar experiments of Blatter et al. (2013) did not produce high-Na dacites because equilibrium (rather than fractional) crystallization produced unrealistically large amounts of Na-bearing amphibole. Although untested, it is conceivable that strictly fractional crystallization could have produced greater Na enrichment in their experiments, so the possibility of deep crustal fractionation leading to Na-Fe-Ti-enriched compositions cannot be completely ruled out. However, such magmas would be significantly Al_2O_3-enriched relative to the TNC due to the aforementioned suppression of plagioclase crystallization. We therefore note that this cannot be the origin of any of the Na-Fe-Ti-enriched compositions mentioned in this paper (including the Shevlin Park Tuff, Three Sisters andesite-dacites and Medicine Lake rim andesites), all of which have Al_2O_3 contents nearly identical to the TNC. To achieve extreme Na-enrichment coupled with FeTi-enrichment requires 1-2 wt.% H_2O in the melt, but for all available data it also appears to require shallow crustal pressures.

It is worth noting here that despite the modest H_2O contents in the TNC and other damp magmas described in this paper, both the TNC and the Shevlin Park Tuff were erupted explosively. These two tuffs are among a limited number of large explosive eruptions documented in the Cascades (Nathenson et al. 2012), and indicate that high initial H_2O contents are not required in the parental magma to produce large explosive eruptions. Progressive

enrichment of H_2O in the melt during fractional crystallization can lead to higher H_2O contents in the derivative silicic magmas, promoting explosive eruption by vapor phase exsolution.

LLDs as tools for determining magmatic H_2O contents

Zimmer et al. (2010) have recently developed a tool for determining magmatic H_2O content to within ~2 wt.% using liquid lines of descent. This tool, termed the "tholeiitic index" (THI = $Fe_{4.0}/Fe_{8.0}$, where $Fe_{4.0}$ = wt.% FeO at 4±1 wt.% MgO, and $Fe_{8.0}$ = wt.% FeO at 8±1 wt.% MgO) is an effective method for the approximation of H_2O content in a magmatic system but is only applicable to LLDs that extend back to primitive basaltic compositions (MgO > 7 wt.%). This limits its utility for many arc suites such as those presented in this paper (the most MgO-rich composition in TNC ~ 4 wt.% MgO; Medicine Lake rim andesites ~ 3 wt.% MgO; Shevlin Park Tuff ~3 wt.% MgO). We have shown here that LLDs provide reliable estimates of magmatic H_2O contents and that they can be used even when very primitive (mafic) compositions are absent.

A final observation that can be made from Fig. 10 is that the Cascade arc contains very few examples of anhydrous lavas that have evolved much beyond primitive, mantle-derived compositions (low SiO_2, high MgO) solely by crystal fractionation. Such lavas should be easily identifiable by strong FeO and TiO_2 enrichment exceeding that of the TNC. Examples of *moderate* FeO and TiO_2 enrichment (FeO/MgO = 2.5 - 3 in the basaltic andesite compositional range) have been described in this paper (TNC pumices etc.; Fig. 10) and elsewhere in the central and northern Oregon Cascades (Conrey et al. 2002). This moderate FeO and TiO_2 enrichment is a result of small-modest amounts of magmatic water. However, extensive fractionation of *anhydrous* magmas is not observed in the Cascades. While small amounts of

anhydrous fractionation may occur, extremely high FeO/MgO (>3.5 in basalts to basaltic andesites) and low Al_2O_3 (<14 wt.%) characteristic of extensive anhydrous fractionation (Carmichael 1964; Hunter and Sparks 1987; Juster et al. 1989) are not observed. This seems surprising at first because *primitive* anhydrous magmas, namely low-K high-alumina olivine tholeiites (HAOT), have been documented at Mt. Shasta (Grove et al. 2002), the Lassen Volcanic Center (Clynne et al. 2008), Medicine Lake volcano (Grove et al. 1988; Donnelly-Nolan et al. 1991), Mt. Mazama (Bacon et al. 1994) and widely throughout the Cascade arc (Smith 1993; Bacon et al. 1997; Conrey et al. 2002; Hildreth 2007). However, in most areas, anhydrous magmas emplaced into the Cascade arc crust seem to erupt without significant crustal residence and differentiation. Those anhydrous magmas that do pond in the crust are very hot and so assimilate the fusible calcalkaline (wet) crustal rocks. This assimilation masks the anhydrous, tholeiitic nature of the original magmas and produces basalts and andesites with calcalkaline compositional features inherited from the assimilated component (e.g. Grove et al. 1988; Baker et al. 1991; Kinzler et al. 2000). As a result, damp fractionation trends that straddle the tholeiitic-calcalkaline transition represent the most strongly tholeiitic fractionation trends preserved in the Cascades, while most arc magmas fall in the calcalkaline range (Fig. 10) due either to wet fractionation (3-6 wt.% H_2O) or assimilation of crustal calcalkaline rocks.

Conclusions

High-Na dacites in the Cascade arc have higher FeO and TiO_2 than typical calcalkaline Cascade lavas. We have shown here that this is due to modest amounts of H_2O in the parental melt (1-2 wt.%). For the tuff of Newberry caldera (TNC), the pre-eruptive conditions of the most mafic (basaltic andesite) liquids preserved were ~1070°C and 1.5 wt.% H_2O. Fractional crystallization

of these liquids under H_2O-undersaturated conditions at upper crustal pressures yielded high-Na dacitic liquids with ~2.8 wt.% H_2O at ~970°C after ~50% fractionation by mass. The rhyolites of the TNC may have been produced by continued fractional crystallization of the high-Na dacitic liquids.

The TNC and the rim andesites at Medicine Lake volcano both record modest H_2O contents. However, modest H_2O contents are not unique to the rear arc, as illustrated by the compositionally similar Shevlin Park Tuff and dacites erupted at the Three Sisters, all from the central Oregon segment of the main Cascade arc axis. Volcanoes at the arc axis and in the rear arc both produce magmas with a wide range of H_2O contents. Despite this complexity, a distinction can be made between the more important role of wet magmas in the southern Cascades and damp magmas in the central Oregon Cascades.

In general, modest H_2O contents produce coupled Na, Fe and Ti enrichment relative to wetter calcalkaline magmas. The relative stabilities of plagioclase and FeTi oxides necessary to produce this compositional feature require a narrow range of H_2O content (1-2 wt.%). This highlights the power and precision of well-constrained LLDs as a tool for determining magmatic H_2O content.

Acknowledgements

We express our gratitude to Rick Conrey for providing data for the Shevlin Park Tuff, Jocelyn Fuentes for experimental and analytical insights into the Medicine Lake rim andesites, James Pershken for assistance with sample preparation, Jean-Arthur Olive for MATLAB wizardry, Neel Chatterjee for assistance with the electron microprobe, and Bob Jensen for field assistance.

Thoughtful reviews from K.D. Putirka, M.N. Brounce, M.R. Perfit and T.W. Sisson led to a stronger manuscript. Our thanks also go to J. Hoefs for editorial handling of this manuscript.

References

Allègre CJ, Treuil M, Minster J-F, Minster B, Albarède F (1977) Systematic use of trace element in igneous process. Part I: Fractional crystallization processes in volcanic suites. Contrib Mineral Petrol 60:57-75.

Almeev RR, Holtz F, Koepke J, Parat F (2012) Experimental calibration of the effect of H_2O on plagioclase crystallization in basaltic melt at 200 MPa. Am Mineral 97:1234-1240.

Anderson AT, Jr. (1979) Water in some hypersthenic magmas. J Geol 87:509-531.

Bacon CR, Gunn SH, Lanphere MA, Wooden JL (1994) Multiple isotopic components in Quaternary volcanic rocks of the Cascade Arc near Crater Lake, Oregon. J Petrol 35:1521-1556.

Bacon CR, Bruggman PE, Christiansen RL, Clynne MA, Donnelly-Nolan JM, Hildreth W (1997) Primitive magmas at five Cascade volcanic fields: melts from hot, heterogeneous sub-arc mantle. Can Mineral 35:397-423.

Baker MB, Grove TL, Kinzler RJ, Donnelly-Nolan JM, Wandless GA (1991) Origin of compositional zonation (high-alumina basalt to basaltic andesite) in the Giant Crater lava field, Medicine Lake Volcano, Northern California. J Geophys Res 96:21819-21842.

Baker MB, Grove TL, Price R (1994) Primitive basalts and andesites from the Mt. Shasta region, N. California: products of varying melt fraction and water content. Contrib Mineral Petrol 118:111-129.

Bartels KS, Kinzler RJ, Grove TL (1991) High pressure phase relations of primitive high-alumina basalts from Medicine Lake volcano, northern California. Contrib Mineral Petrol 108:253-270.

Blatter DL, Sisson TW, Hankins WB (2013) Crystallization of oxidized, moderately hydrous arc basalt at mid- to lower-crustal pressures: implications for andesite genesis. Contrib Mineral Petrol 166:861-886.

Blundy JD, Wood BJ (1991) Crystal-chemical controls on the partitioning of Sr and Ba between plagioclase feldspar, silicate melts, and hydrothermal solutions. Geochim Cosmochim Acta 55:193-209.

Bryan WB, Finger LW, Chayes F (1969) Estimating proportions in petrographic mixing equations by least squares approximation. Science 163:926-927.

Clynne MA, Muffler LJP, Siems DF, Taggart Jr. JE, Bruggman P (2008) Major and EDXRF trace element chemical analyses of volcanic rocks from Lassen Volcanic National Park and vicinity, California. USGS Open-File Report 2008-1091, http://pubs.usgs.gov/of/2008/1091/.

Conrey RM, Hooper PR, Larson PB, Chesley J, Ruiz J (2001) Trace element and isotopic evidence for two types of crustal melting beneath a High Cascade volcanic center, Mt. Jefferson, Oregon. Contrib Mineral Petrol 141:710-732.

Conrey RM, Taylor EM, Donnelly-Nolan JM, Sherrod DR (2002) North-central Oregon Cascades: Exploring petrologic and tectonic intimacy in a propagating intra-arc rift. In: Moore GW (ed) Field guide to geologic processes in Cascadia. Oregon Department of Geology and Mineral Industries Special Paper 36, pp. 47-90.

Danyushevsky LV (2001) The effect of small amounts of H_2O on crystallization of mid-ocean ridge and backarc basin magmas. J Volcanol Geotherm Res 110:265-280.

Dixon JE, Stolper EM, Holloway JR (1995) An experimental study of water and carbon dioxide solubilities in mid-ocean ridge basaltic liquids. Part I: Calibration and solubility models. J Petrol 36:1607-1631.

Donnelly-Nolan JM (2008) Chemical analyses of pre-Holocene rocks from Medicine Lake volcano and vicinity, Northern California. USGS Open-File Report 2008-1094, http://pubs.usgs.gov/of/2008/1094/.

Donnelly-Nolan JM, Champion DE, Grove TL, Baker MB, Taggart JE, Bruggman PE (1991) The Giant Crater lava field: Geology and geochemistry of a compositionally zoned, high-alumina basalt to basaltic andesite eruption at Medicine Lake volcano, California. J Geophys Res 96:21843-21863.

Donnelly-Nolan JM, Grove TL, Lanphere MA, Champion DE, Ramsey DW (2008) Eruptive history and tectonic setting of Medicine Lake Volcano, a large rear-arc volcano in the southern Cascades. J Volcanol Geotherm Res 177:313-328.

Donnelly-Nolan JM, Stovall WK, Ramsey DW, Ewert JW, Jensen RA (2011) Newberry Volcano – central Oregon's sleeping giant. USGS Fact Sheet 2011-3145, http://pubs.usgs.gov/fs/2011/3145/.

Eggler DH (1972) Water-saturated and undersaturated melting relations in a Paricutin andesite and an estimate of water content in the natural magma. Contrib Mineral Petrol 34:261-271.

Elkins LT, Grove TL (1990) Ternary feldspar experiments and thermodynamic models. Am Mineral 75:544-559.

Ewart A (1979) A review of the mineralogy and chemistry of Tertiary-Recent, dacitic, latitic, rhyolitic and related silicic rocks. In: Barker F (ed) Trondhjemites, dacites and related rocks. Elsevier, Amsterdam, pp. 13-121.

Ewart A (1982) The mineralogy and petrology of Tertiary-Recent orogenic volcanic rocks: with special reference to the andesitic-basaltic compositional range. In: Thorpe RS (ed) Andesites: Orogenic andesites and related rocks. Wiley, New York, pp. 25-95.

Falloon TJ, Danyushevsky LV (2000) Melting of refractory mantle at 1.5, 2 and 2.5 GPa under anhydrous and H_2O-undersaturated conditions: implications for the petrogenesis of high-Ca boninites and the influence of subduction components on mantle melting. J Petrol 41:257-283.

George R, Turner S, Hawkesworth C, Bacon CR, Nye C, Stelling P, Dreher S (2004) Chemical versus temporal controls on the evolution of tholeiitic and calc-alkaline magmas at two volcanoes in the Alaska-Aleutian arc. J Petrol 45:203-219.

Grove TL, Bryan WB (1983) Fractionation of pyroxene-phyric MORB at low pressure: An experimental study. Contrib Mineral Petrol 1983:293-309.

Grove TL, Baker MB (1984) Phase equilibrium controls on the calc-alkaline vs. tholeiitic differentiation trends. J Geophys Res 89:3253-3274.

Grove TL, Juster TC (1989) Experimental investigations of low-Ca pyroxene stability and olivine-pyroxene-liquid equilibria at 1-atm in natural basaltic and andesitic liquids. Contrib Mineral Petrol 103:287-305.

Grove TL, Donnelly-Nolan JM, Housh T (1997) Magmatic processes that generated the rhyolite of Glass Mountain, Medicine Lake volcano, N California. Contrib Mineral Petrol 127:205-223.

Grove TL, Kinzler RJ, Baker MB, Donnelly-Nolan JM, Lesher CE (1988) Assimilation of granite by basaltic magma at Burnt Lava flow, Medicine Lake volcano, northern California: Decoupling of heat and mass transfer. Contrib Mineral Petrol 99:320-343.

Grove TL, Parman SW, Bowring SA, Price RC, Baker MB (2002) The role of an H_2O-rich fluid component in the generation of primitive basaltic andesites and andesites from the Mt. Shasta region, N. California. Contrib Mineral Petrol 142:375-396.

Grove TL, Baker MB, Price RC, Parman SW, Elkins-Tanton LT, Chatterjee N, Müntener O (2005) Magnesian andesite and dacite lavas from Mt. Shasta, northern California: products of fractional crystallization of H_2O-rich mantle melts. Contrib Mineral Petrol 148:542-565.

Hess PC (1992) Phase equilibria constraints on the origin of ocean floor basalts. In: Morgan JP, Blackman DK, Sinton JM (eds) Mantle flow and melt generation at mid-ocean ridges. Geophysical Monograph 71:67-102.

Hildreth W (2007) Quaternary magmatism in the cascades – Geologic perspectives. U.S. Geological Survey Professional Paper 1744, 125 pp., http://pubs.usgs.gov/pp/pp1744/.

Hildreth W, Fierstein J, Calvert AT (2012) Geologic map of the Three Sisters volcanic cluster. USGS Scientific Investigations Map, scale 1:24,000, http://pubs.usgs.gov/sim/3186/.

Hunter RH, Sparks RSJ (1987) The differentiation of the Skaergaard Intrusion. Contrib Mineral Petrol 95:451-461.

Jensen RA, Donnelly-Nolan JM, Mckay D (2009) A field guide to Newberry Volcano, Oregon. In: O'Conner JE, Dorsey RJ, Madin IP (eds) Volcanoes to vineyards: Geologic field trips through the dynamic landscape of the Pacific Northwest. Geol Soc Am Field Guide 15, pp. 53-79.

Jicha BR, Hart GL, Johnson CM, Hildreth W, Beard BL, Shirey SB, Valley JW (2009) Isotopic and trace element constraints on the petrogenesis of lavas from the Mount Adams volcanic field, Washington. Contrib Mineral Petrol 157:189-207.

Johnson MC, Anderson AT Jr., Rutherford MJ (1994) Pre-eruptive volatile contents of magmas. In: Carroll MR, Holloway JR (eds) Volatiles in Magmas. Reviews in Mineralogy 30, pp. 281-330.

Johnson RW, Arculus RJ (1978) Volcanic rocks of the Witu Islands, Papua New Guinea: The origin of magmas above the deepest part of the New Britain Benioff zone. Bull Volcanol 41:609-655.

Juster TC, Grove TL, Perfit MR (1989) Experimental constraints on the generation of FeTi basalts, andesites and rhyodacites at the Galapagos spreading center, 85°C and 95°W. J Geophys Res 94:9251-9274.

Kelemen PB, Rilling JL, Parmentier EM, Mehl L, Hacker BR (2003) Thermal structure due to solid-state flow in the mantle wedge beneath arcs. In: Eiler JM (ed) Inside the subduction factory. Geophysical Monograph 138:293-311.

Kelley KA, Plank T, Grove TL, Stolper EM, Newman S, Hauri E (2006) Mantle melting as a function of water content beneath back-arc basins. J Geophys Res 111:B09208.

Kinzler RJ, Donnelly-Nolan JM, Grove TL (2000) Late Holocene hydrous mafic magmatism at the Paint Pot Crater and Callahan flows, Medicine Lake Volcano, N. California and the influence of H_2O in the generation of silicic magmas. Contrib Mineral Petrol 138:1-16.

Krawczynski MJ, Grove TL, Behrens H (2012) Amphibole stability in primitive arc magmas: effects of temperature, H_2O content, and oxygen fugacity. Contrib Mineral Petrol 164:317-339.

Lange RA, Frey HM, Hector J (2009) A thermodynamic model for the plagioclase-liquid hygrometer/thermometer. Am Mineral 94:494-506.

Langmuir CH, Bézos A, Escrig S, Parman SW (2006) Chemical systematics and hydrous melting of the mantle in back-arc basins. In: Christie DM, Fisher CR, Lee S-M, Givens S (eds) Back-arc spreading systems: geological, biological, chemical, and physical interactions. Geophysical Monograph 166:87-146.

Lesne P, Scaillet B, Pichavant M, Iacono-Marziano G, Beny J-M (2011) The H_2O solubility of alkali basaltic melts: an experimental study. Contrib Mineral Petrol 162:133-151.

MacLeod NS, Sherrod DR, Chitwood LA, Jensen RA (1995) Geologic map of Newberry volcano, Deschutes, Klamath, and Lake Counties, Oregon: U.S. Geological Survey Miscellaneous Geologic Investigations Map I-2455, http://pubs.usgs.gov/imap/2455/.

Médard E, Grove TL (2008) The effect of H_2O on the olivine liquidus of basaltic melts: experiments and thermodynamic models. Contrib Mineral Petrol 155:417-432.

Miyashiro A (1974) Volcanic rock series in island arcs and active continental margins. Am J Sci 274:321-355.

Moore G, Vennemann T, Carmichael ISE (1998) An empirical model for the solubility of H_2O in magmas to 3 kilobars. Am Mineral 83:36-42.

Nandedkar RH, Ulmer P, Müntener O (2014) Fractional crystallization of primitive, hydrous arc magmas: an experimental study at 0.7 GPa. Contrib Mineral Petrol 167:1015.

Nathenson M, Clynne MA, Muffler, LJP (2012) Eruption probabilities for the Lassen Volcanic Center and regional volcanism, northern California, and probabilities for large explosive eruptions in the Cascade Range. U.S. Geological Survey Scientific Investigations Report 2012-5176-B, 23 pp., http://pubs.usgs.gov/sir/2012/5176/b/.

Parman SW, Grove TL, Kelley KA, Plank T (2011) Along-arc variations in the pre-eruptive H_2O contents of Mariana Arc magmas inferred from fractionation paths. J Petrol 52:257-278.

Plank T, Kelley KA, Zimmer MM, Hauri EH, Wallace PJ (2013) Why do mafic arc magmas contain ~4 wt% water on average? Earth Planet Sci Lett 364:168-179.

Putirka KD (2008) Thermometers and barometers for volcanic systems. In: Putirka KD, Tepley III FJ (eds) Minerals, Inclusions and Volcanic Processes. Reviews in Mineralogy and Geochemistry 69, pp.61-120.

Ratajeski K, Sisson TW (1999) Loss of iron to gold capsules in rock-melting experiments. Am Mineral 84:1521-1527.

Rollinson HR (1993) Using geochemical data: Evaluation, presentation, interpretation. Longman, UK. 352 pp.

Schmidt ME, Grunder AL, Rowe MC (2008) Segmentation of the Cascade arc as indicated by Sr and Nd isotopic variation among diverse primitive basalts. Earth Planet Sci Lett 266:166-181.

Sisson TW, Grove TL (1993) Experimental investigations of the role of H_2O in calc-alkaline differentiation and subduction zone magmatism. Contrib Mineral Petrol 113:143-166.

Sisson TW, Layne GD (1993) H_2O in basalt and basaltic andesite glass inclusions from four subduction-related volcanoes. Earth Planet Sci Lett 117:617-639.

Smith JG (1993) Geologic map of upper Eocene to Holocene volcanic and related rocks in the Cascade Range, Washington. U.S. Geological Survey Map I-2005, scale 1:500,000.

Stolper E, Newman S (1994) The role of water in the petrogenesis of Mariana trough magmas. Earth Planet Sci Lett 121:293-325.

Tatsumi Y, Sakuyama M, Fukuyama H, Kushiro I (1983) Generation of arc basalt magmas and thermal structure of the mantle wedge in subduction zones. J Geophys Res 88:5815-5825.

Till CB, Grove TL, Carlson RW, Fouch MJ, Donnelly-Nolan JM, Wagner LS, Hart WK (2013) Depths and temperatures of <10.5 Ma mantle melting and the lithosphere-asthenosphere boundary below southern Oregon and northern California. Geochem Geophys Geosyst 14:864-879.

Van Orman JA, Grove TL, Shimizu N (2001) Rare earth element diffusion in diopside: influence of temperature, pressure, and ionic radius, and an elastic model for diffusion in silicates. Contrib Mineral Petrol 141:687-703.

Villiger S, Ulmer P, Müntener O, Thompson AB (2004) The liquid line of descent of anhydrous, mantle-derived, tholeiitic liquids by fractional and equilibrium crystallization – an experimental study at 1.0 GPa. J Petrol 45:2369-2388.

Villiger S, Ulmer P, Müntener O (2007) Equilibrium and fractional crystallization experiments at 0.7 GPa; the effect of pressure on phase relations and liquid compositions of tholeiitic magmas. J Petrol 48:159-184.

Yoder HS, Tilley CE (1962) Origin of basalt magmas: An experimental study of natural and synthetic rock systems. J Petrol 3:342-532.

Zimmer MM, Plank T, Hauri EH, Yogodzinski GM, Stelling P, Larsen J, Singer B, Jicha B, Mandeville C, Nye CJ (2010) The role of water in generating the calc-alkaline trend: New volatile data for Aleutian magmas and a new tholeiitic index. J Petrol 51:2411-2444.

Figure Captions

Fig. 1 Shaded relief map of the NW United States showing the locations of major Cascade volcanoes (filled triangles). Highlighted is Newberry Volcano, a major rear-arc volcanic center east of the main arc. Adapted from Donnelly-Nolan et al. (2008)

Fig. 2 Lidar image of Newberry Volcano. Caldera rim is outlined in black; black circles show sample locations for the tuff of Newberry caldera. Open circles are sample locations for starting materials for experiments (692Ja & 272Ja). Inset: larger-scale map; white outline shows the full extent of lava flows from Newberry Volcano (adapted from Donnelly-Nolan et al., 2011)

Fig. 3 Major-element variation diagrams showing the range of pumice compositions in the TNC, plus representative samples of similar basaltic andesites erupted just before the caldera-forming eruption (open diamonds; Table 1). Pumices 692Ja and 272Ja, studied in detail and used as experimental starting materials, are highlighted in gray. Tholeiitic-calcalkaline dividing line from Miyashiro (1974)

Fig. 4 Back-scattered electron images of glomerocrysts in selected TNC pumices. (A) Top row shows two glomerocrysts in sample 692Ja. They are in equilibrium with the bulk composition, indicating multiple saturation with olivine (ol), plagioclase (plag), clinopyroxene (cpx) and an FeTi oxide (ox). (B) Bottom row shows two glomerocrysts in the high-Na pumices from the 272Ja site. These pumices are multiply saturated in plagioclase (plag), orthopyroxene (opx), apatite (ap) and two FeTi oxides (ox)

Fig. 5 Figure showing how low-Na_2O, high-Al_2O_3 pumices associated with but distinct from the TNC (open circles) form a compositional trend that cannot result from mixing between low- and high-SiO_2 liquids from the main TNC trend (shaded field). These low-Na_2O pumices represent a small, discrete batch of magma erupted just prior to the main TNC magmas

Fig. 6 Major-element variation diagrams showing experimental liquids (bold symbols) overlain on TNC pumice compositions (gray circles). The two 1 kbar experiments performed on composition 272Ja are labeled in the top-left diagram. 1 kbar H_2O-saturated experiments best reproduce the TNC liquids but are still slightly too H_2O-rich (see text)

Fig. 7 Experimental H_2O-saturated ($P_{H_2O} = P_{total}$) phase diagram for sample 692Ja. Grey field = olivine present. Multiple saturation in the four phenocryst phases found in the natural sample 692Ja occurs near 0.4 kbar H_2O-saturated conditions, corresponding to an H_2O content of ~1.5 wt.%

Fig. 8 Figure showing the effect of H_2O on bulk crystal composition and the resulting compositional evolution of residual liquids in experiments on sample 692Ja (55.9 wt.% SiO_2). Colored diamonds show the bulk crystal composition for experiments at 1 bar (run 1: 0% H_2O in the melt, red), 1 kbar (run 38a, ~3% H_2O, light blue) and 2 kbar (run 26, ~6% H_2O, dark blue). Arrows are color-coded to show the compositional evolution of the liquid resulting from crystallization of these assemblages. The suite of elemental trends in the TNC pumices can only be reproduced by a narrow range of low H_2O contents (1-2 wt.%) – see text for details

Fig. 9 Modeled effects of fractional crystallization (solid line) vs. equilibrium crystallization (dashed line) on Ba and Rb concentrations in the evolving TNC liquid. See Table 6 for model details

Fig. 10 Major element variation diagrams showing compositional features of the TNC (open circles) compared to compositionally similar volcanic rocks (filled circles), and analyses from other volcanic centers (shaded fields) in the central and southern Cascades. The Shevlin Park Tuff and Medicine Lake rim andesites, plus some lava flows from the Three Sisters, are all compositionally similar to the TNC. The major southernmost Cascade volcanoes, Lassen and Mt. Shasta, are distinctly different, while the rear-arc Medicine Lake volcano (California) and arc-axis Three Sisters (Oregon) erupt a range of magma types, from TNC-like to Lassen-like. Shaded fields represent large databases from individual volcanic centers, including every analysis that yielded a major element total of 98.5 – 101.5 wt.%. Some rhyolites at Newberry and Medicine Lake extend to FeO/MgO > 8 and so are not shown in (c). Isolated point from Mt. Shasta at 70 wt.% SiO_2 is a single analysis. See supplementary files for TNC, Shevlin Park Tuff and Medicine Lake rim andesite data. Other data sources: Lassen – 439 analyses from Clynne et al. (2008); "Other" Medicine Lake – 268 analyses from Donnelly-Nolan (2008); Three Sisters – 603 analyses from Hildreth et al. (2012); Shasta – 75 analyses from Baker et al. (1994), Grove et al. (2002) and Grove et al. (2005); "Other" Newberry – 686 analyses from J.M. Donnelly-Nolan (unpublished data). Tholeiitic-calcalkaline dividing line in (c) from Miyashiro (1974)

Table Captions

Table 1 Representative major and trace element data for pumices in the tuff of Newberry caldera, plus pre-caldera lavas thought to be genetically related to TNC pumices. All analyses normalized to totals of 100 based on FeO. 1-sigma standard errors are < 1% for major elements, < 5% for minor and trace elements

Table 2 Make-up of seed mix for seeded experiments on 692Ja

Table 3 Experimental conditions and products

Table 4 Electron microprobe analyses of experimental phases. Values are in weight percent. Numbers in parentheses are 1 standard deviation of replicate analyses in terms of last unit given (e.g. 59.3(5) = 59.3 ± 0.5). Hydrous glass analyses are renormalized to 100, with original totals displayed in the "Total" column. All Fe is given as FeO. n = number of analyses

Table 5 Comparison of calculated liquidus temperatures for 692Ja at different P-H2O conditions. All thermometers are calibrated using both anhydrous and hydrous liquids but are grouped according to whether or not they have an H2O term in their calculation.

Table 6 Rb-Ba fractional vs. equilibrium crystallization model

Table 7 Inputs and results of crystallization model for high-Na trend

Table 1 Representative major and trace element data for pumices in the tuff of Newberry caldera, plus pre-caldera lavas thought to be genetically related to
TNC pumices. All analyses normalized to totals of 100 based on FeO. 1-sigma standard errors are < 1% for major elements, < 5% for minor and trace elements

High-Na	Low-Na	Pre-caldera lavas

Sample	205J	692Ja	923J	271Jc	1085Ja	272Ja	271Ja	836Ja	1788Jb	1786Jc	933Ja1	1809JI3	1809JI1	1102Jg	1102Jf	1700J	943J
SiO_2	53.3	55.9	57.8	60.4	63.1	66.3	66.5	69.5	70.5	71.9	73.9	53.9	55.0	61.9	62.9	51.8	53.2
TiO_2	2.18	2.16	1.87	1.55	1.25	0.90	0.86	0.53	0.38	0.29	0.23	2.20	2.21	0.90	0.91	2.17	2.14
Al_2O_3	16.0	16.1	16.1	16.0	15.9	15.7	15.6	15.3	15.1	14.8	14.0	17.1	16.7	16.7	16.6	16.2	15.9
FeO	10.9	9.48	8.53	6.95	5.89	4.59	4.50	3.38	3.73	3.11	1.83	11.3	11.1	5.98	5.84	11.2	10.7
MnO	0.19	0.19	0.20	0.17	0.17	0.15	0.15	0.10	0.13	0.10	0.05	0.19	0.19	0.14	0.14	0.19	0.18
MgO	4.02	3.22	2.70	2.33	1.78	1.09	1.03	0.60	0.34	0.18	0.21	3.48	3.24	2.96	2.30	4.55	4.11
CaO	7.99	6.65	5.86	4.89	3.95	2.67	2.56	1.86	1.60	1.10	0.95	6.92	6.60	5.25	4.98	8.73	8.11
Na_2O	4.23	4.79	5.15	5.59	5.81	6.38	6.58	5.59	5.50	4.96	4.57	3.67	3.65	3.95	3.95	4.18	4.40
K_2O	0.81	1.01	1.23	1.36	1.57	1.88	1.92	3.00	2.66	3.50	4.21	0.80	0.91	1.89	2.09	0.62	0.80
P_2O_5	0.43	0.52	0.60	0.76	0.60	0.34	0.32	0.17	0.38	0.04	0.04	0.39	0.43	0.31	0.27	0.39	0.45
Mg#	39.8	37.7	36.0	37.4	35.0	29.8	29.0	24.1	14.0	9.5	17.0	35.4	34.3	46.9	41.2	42.0	40.7
Rb	16	17	19	27	29	38	39	79	52	82	120	18	20	44	45	9	11
Sr	143	424	406	433	370	274	267	176	145	80	61	428	428	297	292	431	441
Y	31	40	40	44	40	44	45	45	49	59	41	44	45	35	-	33	31
Zr	114	169	192	197	229	258	263	337	305	351	267	155	154	211	-	143	142
Nb	13	11	11	13	11	15	15	18	13	19	15	12	12	10	-	11	8
Ba	310	353	440	446	590	589	664	840	740	779	830	427	440	647	678	281	304
Ni	15	10	3	<2	3	4	3	4	1	1	4	0	4	20	6	18	<4
Cu	76	10	2	3	2	2	4	4	10	9	6	40	34	29	28	75	59
Zn	94	108	97	104	93	97	100	75	94	80	42	108	108	76	72	104	83
Cr	-	<5	<5	<3	<5	8	8	6	3	3	6	4	5	<5	-	25	<5
Ce	-	32	45	43	47	43	41	60	52	67	58	34	37	41	44	28	26
Ga	-	23	17	21	16	24	22	21	21	22	18	23	20	14	15	21	17
La	-	14	11	20	20	19	21	32	24	33	33	16	17	17	15	11	9
Nd	-	25	21	35	36	28	33	36	27	31	24	26	25	37	16	23	12
V	-	198	150	115	57	39	36	17	4	7	7	291	259	<5	-	330	313

All samples analyzed at the USGS except 933Ja1, 1700J, 1786Jc, 1788Jb, 1809JI1, 1809J3, analyzed at WSU. See supplementary information for analytical methods.

Table 2 Make-up of seed mix for seeded experiments on 692Ja

	Mineral compositions									
	Quartz*	Albite[1]	Bytown-ite[1]	Micro-cline[1]	Kuhnlun diopside[2]	Kragero opx[3]	Fayalite*	TiO_2*	Apatite*	Bulk
SiO_2	100	68.6	50.2	65.9	55.8	57.3	29.5	0	0	56.11
TiO_2	0	0	0	0	0.04	0.06	0	52.6	0	2.16
Al_2O_3	0	19.4	32.5	18.9	0.88	0.1	0	0	0	16.14
FeO	0	0	0.42	0	0.7	9.49	70.5	47.4	0	9.78

MnO	0	0	0	0	0.05	0.14	0	0	0	0.01
MgO	0	0	0	0	17.7	33.5	0	0	0	3.21
CaO	0	0.02	15.3	0	24.5	0.26	0	0	55.6	6.56
Na_2O	0	11.8	2.68	3.36	0.48	0	0	0	0	4.86
K_2O	0	0.16	0.07	11.7	0	0	0	0	0	0.99
P_2O_5	0	0	0	0	0	0	0	0	42.2	0.51
Proportion	0.05	0.33	0.25	0.08	0.08	0.05	0.10	0.04	0.01	

*Quartz, fayalite and apatite are synthetic, produced from spec-pure oxides. TiO_2 is spec-pure oxide.

[1]Albite, bytownite and microcline compositions from Elkins & Grove (1990).

[2]Kuhnlun diopside composition from Van Orman et al. (2001).

[3]Kragero opx composition from Grove & Juster (1989).

Table 3 Experimental conditions and products

Run #	T (°C)	P (kbar)	Time (hours)	Phases (+ vapor)	ΣFeO*	ΣR²	K_D ol/liq	K_D cpx/liq	K_D pig/liq	K_D opx/liq	K_D plag/liq	K_D amph/liq
692Ja-5	1170	0.001	21	gl (100)	0							
692Ja-6	1150	0.001	18	gl (97), plag (3)	4.5						1.57	
692Ja-4	1120	0.001	17	gl (86), ol (tr), plag (14)	5.1						1.40	
692Ja-1	1070	0.001	120	gl (43), il (1), mt (3), cpx (6), pig (5), plag (42)	0.1						1.00	
692Ja-2	1050	0.001	168	gl (29), il (1), mt (4), cpx (10), pig (6), plag (50)	0				0.22		1.00	
692Ja-43	1000	1	30	gl (94), il (0), mt (3), cpx (3)	0.1	0.06		0.26				
692Ja-46	985	1	33	gl (92), il (1), mt (2), cpx (5)	0.2	0.13		0.22				
692Ja-29	970	1	48	gl (69), il (1), mt (4), cpx (7), ol (3), plag (15), ap (1)	0	0.01	0.30	0.23			2.63	
692Ja-38a	950	1	51	gl (54), il (2), mt (5), cpx (7), ol (4), plag (26), ap (2)	0	0.03	0.27	0.31			4.07	
692Ja-45	935	1	45	gl (54), il (2), mt (5), cpx (8), ol (4), plag (25), ap (2)	0	0.00	0.28	0.20			3.45	
272Ja-1	920	1	47	gl (92), il (tr), mt (2), cpx (-4), opx (4), plag (5), ap (1)	-0.1	0.78		0.21		0.26	3.27	
272Ja-2b	900	1	71	gl (84), il (tr), mt (2), cpx (-4), opx (5), plag (11), ap (2)	-0.2	0.47		0.19		0.21	3.23	
692Ja-23	1000	2	25	gl (100)	0							
692Ja-24	970	2	46	gl (92), il (1), mt (2), cpx (4)	0.1	0.22		0.22				
692Ja-25	950	2	47	gl (84), il (1), mt (3), cpx (3), amph (9)	0.1	0.46		0.21				0.31
692Ja-26	935	2	72	gl (79), il (1), mt (3), cpx (-1), amph (17), ap (1)	0	0.10		0.20				0.28

gl = glass; *il* = ilmenite; *mt* = magnetite; *cpx* = clinopyroxene *ol* = olivine; *plag* = plagioclase; *ap* = apatite; *amph* = amphibole; *pig* = pigeonite

All experiments on sample 692Ja except two on 272Ja noted in Run #.

All pyroxenes denoted *cpx* are high-Ca cpx to distinguish from pigeonite found in some 1-bar runs.
*Change in FeO in relative percent (i.e. for a bulk starting composition with 10% FeO, a bulk final product with 10.5% FeO would have ΣFeO = 5).

Table 4 Electron microprobe analyses of experimental phases. Values are in weight percent. Numbers in parentheses are 1 standard deviation of replicate analyses in terms of last unit given (i.e. 59.3(5) = 59.3 ± 0.5). Hydrous glass analyses are renormalized to 100 and all Fe is given as FeO. n = number of analyses.

Run No.	Phase	n	SiO_2	TiO_2	Al_2O_3	FeO	MnO	MgO	CaO	Na_2O	K_2O	P_2O_5	Total
692Ja-5	gl	9	55.1(2)	2.49(12)	15.5(1)	10.4(1)	0.20(3)	3.40(6)	6.65(6)	4.7(1)	0.88(2)	0.46(5)	99.8
692Ja-6	gl	13	54.7(4)	2.4(2)	15.6(2)	10.0(4)	0.19(4)	3.39(9)	6.76(9)	4.7(1)	0.86(2)	0.44(4)	99.0
	plag	6	54.1(2)		27.9(4)	0.99(20)		0.21(10)	11.3(2)	5.0(1)	0.18(3)		99.6
692Ja-4	gl	15	54.8(4)	2.8(2)	14.2(2)	11.6(4)	0.19(2)	3.85(7)	6.32(12)	4.7(2)	0.98(3)	0.53(7)	99.9
	plag	6	55.8(2)		26.6(5)	1.37(13)		0.27(5)	10.4(1)	5.5(1)	0.20(1)		100.2
692Ja-1	gl	10	59.3(5)	2.8(1)	12.8(2)	10.9(3)	0.18(2)	2.67(7)	5.2(2)	4.5(1)	1.47(3)	0.84(6)	100.6
	plag	6	59.4(9)		24.7(7)	1.17(15)		0.38(9)	7.6(9)	6.7(3)	0.38(4)		100.1
	mt	14	0.34(10)	18.5(9)	2.49(5)	67.9(7)	0.49(4)	3.9(2)					93.7
692Ja-2	gl	10	62.7(4)	2.11(5)	12.9(1)	9.5(3)	0.15(2)	1.87(4)	4.2(1)	4.4(2)	2.03(5)	1.14(5)	100.9
	pig	6	52.7(3)	0.39(2)	0.56(12)	21.8(3)	0.77(2)	19.5(2)	4.3(4)	0.14(3)	0.02(0)		100.2
	plag	11	59.9(4)		24.2(4)	1.03(7)		0.10(5)	6.9(2)	7.2(1)	0.50(2)		99.8
	mt	9	0.32(7)	20.1(3)	2.11(5)	68.1(2)	0.54(5)	3.0(1)					94.2
692Ja-43	gl	15	58.0(5)	1.83(3)	16.8(1)	7.5(1)	0.16(1)	2.9(1)	6.28(8)	5.0(1)	1.00(1)	0.54(4)	95.7
	cpx	21	51.0(6)	1.0(2)	2.7(5)	9.6(4)	0.29(3)	14.3(5)	20.5(5)	0.36(4)	0.02(1)		99.8
	il	6	0.11(4)	44.8(4)	0.48(3)	45.4(4)	0.42(4)	6.0(1)					97.2
	mt	9	0.06(2)	14.9(2)	3.7(1)	72.1(3)	0.48(5)	4.7(2)					95.9
692Ja-46	gl	16	58.3(3)	1.52(3)	17.0(1)	7.68(7)	0.17(1)	2.5(1)	5.99(6)	5.3(2)	1.04(2)	0.42(7)	96.1
	cpx		51.6(6)	1.0(2)	2.5(5)	9.9(4)	0.33(3)	15.0(4)	20.5(4)	0.35(4)	0.02(1)		101.1
	il	8	0.2(1)	46.7(4)	0.41(4)	43.6(2)	0.50(4)	5.5(2)					96.9
	mt	11	0.12(2)	16.6(2)	3.69(7)	70.1(2)	0.50(3)	4.26(5)					95.2
692Ja-29	gl	8	62.8(3)	1.08(3)	17.0(2)	5.60(5)	0.14(1)	1.73(3)	4.20(8)	5.7(2)	1.34(2)	0.43(4)	96.9
	ol	5	36.5(3)	0.14(8)	0.03(2)	31.0(8)	0.64(2)	31.7(3)	0.22(2)				100.2
	cpx	10	51.6(6)	0.8(1)	2.1(4)	10.7(3)	0.40(2)	14.3(4)	19.9(4)	0.34(7)	0.02(1)		100.2
	plag	9	55.7(5)		27.7(5)	0.9(1)		0.13(7)	10.3(4)	5.3(2)	0.14(2)		100.1
	il	3	0.3(1)	46.2(4)	0.41(1)	43.7(1)	0.57(2)	4.8(2)					95.9
	mt	9	0.28(5)	15.6(2)	3.4(3)	70.1(3)	0.52(3)	3.4(1)					93.3
692Ja-38a	gl	12	67.4(5)	0.57(4)	16.4(3)	3.74(9)	0.09(3)	1.25(8)	2.59(9)	6.3(2)	1.49(6)	0.26(4)	96.1
	ol	4	37.2(5)	0.12(1)	0.08(8)	27.8(3)	0.81(4)	34.3(3)	0.21(2)				100.5
	cpx	20	51.6(7)	0.6(1)	1.9(4)	12.4(6)	0.42(5)	13.1(6)	19.6(5)	0.36(7)	0.04(1)		100.1
	plag	8	56.6(5)		27.1(6)	0.7(1)		0.09(5)	9.5(2)	5.6(2)	0.16(2)		99.8
	il	5	0.3(2)	43.7(9)	0.43(5)	46.1(5)	0.67(6)	5.3(2)					96.6
	mt	5	0.14(5)	12.0(3)	3.24(9)	75.2(2)	0.66(4)	4.0(1)					95.3
692Ja-45	gl	6	67.2(4)	0.68(6)	16.5(1)	3.9(1)	0.11(2)	0.96(4)	2.68(7)	5.9(2)	1.83(4)	0.30(7)	97.2

	ol	10	36.0(5)	0.1(1)	0.02(1)	33.6(3)	0.87(5)	29.9(3)	0.19(2)				100.7
	cpx	6	51.6(9)	0.9(4)	2.8(8)	11.8(3)	0.48(6)	14.3(5)	18.8(5)	0.43(8)	0.04(3)		101.1
	plag	5	56.5(3)		27.5(4)	0.8(1)		0.06(3)	9.6(2)	6.11(6)	0.16(2)		100.7
	il	7	0.2(2)	46.9(4)	0.31(6)	44.7(2)	0.72(5)	4.5(2)					97.4
	mt	12	0.14(2)	15.0(3)	2.76(6)	73.1(2)	0.64(2)	3.05(5)					94.6
272Ja-1	gl	15	69.6(7)	0.61(4)	16.0(2)	2.98(8)	0.13(1)	0.72(3)	2.04(5)	5.7(2)	1.98(4)	0.16(3)	96.8
	cpx	5	53.3(8)	0.50(12)	1.72(67)	12.2(4)	0.80(6)	14.0(5)	18.0(7)	0.37(13)	0.06(5)		101.0
	opx	6	52.7(4)	0.27(5)	0.52(18)	22.4(2)	1.37(5)	20.6(3)	1.63(4)	0.04(5)	0.03(1)		99.5
	plag	6	58.8(7)		25.9(4)	0.55(4)		0.04(2)	8.0(5)	6.9(2)	0.21(3)		100.3
272Ja-2b	gl	16	70.4(6)	0.47(6)	15.7(2)	2.97(5)	0.10(1)	0.56(6)	1.68(3)	5.9(2)	2.13(4)	0.12(3)	96.2
	cpx	4	52.3(7)	0.59(24)	1.70(61)	13.3(8)	0.86(6)	13.3(8)	17.8(5)	0.38(11)	0.05(1)		100.3
	opx	9	53.3(7)	0.25(4)	0.54(8)	22.6(3)	1.35(4)	20.5(3)	1.71(11)	0.05(2)	0.01(1)		100.3
	plag	6	59.9(4)		24.6(4)	0.58(5)		0.07(5)	6.9(2)	7.4(2)	0.29(2)		99.8
692Ja-23	gl	9	55.8(7)	2.21(4)	16.34(9)	9.5(1)	0.16(1)	3.31(4)	6.57(6)	4.85(8)	0.86(1)	0.45(3)	92.2
692Ja-24	gl	9	58.4(2)	1.44(3)	16.99(5)	7.93(4)	0.14(1)	2.73(4)	6.04(4)	4.93(6)	0.92(1)	0.46(4)	93.2
	il	9	0.19(2)	45.8(4)	0.37(2)	43.4(3)	0.46(5)	5.1(1)					95.4
	mt	6	0.18(3)	14.9(4)	3.3(3)	71.0(5)	0.44(2)	3.7(2)					93.5
	cpx	6	52.1(4)	0.9(1)	2.4(3)	9.2(3)	0.28(3)	14.5(3)	21.3(4)	0.37(5)	0.02(1)		100.9
692Ja-25	gl	10	60.6(4)	1.14(4)	17.5(2)	6.56(3)	0.12(1)	1.94(2)	5.58(9)	5.1(1)	0.98(2)	0.40(2)	92.9
	il	4	0.20(2)	45.7(3)	0.36(2)	42.6(2)	0.57(5)	4.80(8)					94.2
	mt	7	0.26(2)	14.9(1)	3.41(7)	69.4(4)	0.50(2)	3.3(2)					91.9
	cpx	6	51.8(7)	0.8(1)	2.4(4)	9.7(3)	0.30(2)	13.89(9)	21.2(4)	0.32(6)	0.02(1)		100.4
	amph	7	42.7(8)	2.7(4)	10.6(5)	13.9(5)	0.27(2)	13.2(5)	10.6(7)	2.8(2)	0.26(2)		97.1
692Ja-26	gl	13	62.6(5)	0.91(2)	17.9(2)	5.52(9)	0.12(1)	1.39(3)	5.13(9)	5.1(2)	1.01(2)	0.29(5)	94.2
	il	8	0.26(3)	45.6(3)	0.37(3)	44.93(8)	0.63(3)	3.9(2)					95.7
	mt	12	0.28(3)	14.1(3)	3.4(2)	71.3(7)	0.55(3)	2.7(1)					92.4
	cpx	7	51.1(5)	0.78(9)	2.7(4)	10.6(2)	0.34(3)	13.4(3)	21.7(2)	0.36(4)	0.01(1)		100.9
	amph	8	41.9(6)	3.4(3)	11.4(4)	14.6(3)	0.26(2)	13.1(2)	10.7(3)	2.84(9)	0.25(2)		98.5

gl = glass, *plag* = plagioclase, *mt* = magnetite, *pig* = pigeonite, *cpx* = clinopyroxene, *il* = ilmenite, *ol* = olivine, *opx* = orthopyroxene *amph* = amphibole.

Table 5 Comparison of calculated liquidus temperatures for 692Ja at different P-H_2O conditions. All thermometers are calibrated using both anhydrous and hydrous liquids but are grouped according to whether or not they have an H_2O term in their calculation. See text for further details.

Inputs		Liquidus T (°C) for 692Ja															
		No H_2O term		H_2O term										Average temperatures			
P (kbar)	H_2O (wt. %)	13[1]	16	14	15	22	21	23	23sat	24a	26	33	34	No H_2O term	H_2O term	ΔT (°C)	Intercept[2]
1	0	1079	1061	1085	1089	1081	1061	1132	1141	1134	1148	1065	1087	1070	1102	-32	
	1	1078	1061	1073	1074	1064	1045	1090	1100	1099	1114	1053	1073	1070	1079	-9	1069°C

	2	1077	1061	1062	1060	1048	1029	1051	1060	1066	1082	1040	1059	1069	1056	13	1.4 wt.%
	3	1077	1061	1050	1045	1033	1014	1014	1023	1035	1051	1028	1046	1069	1034	35	
2	0	1079	1069	1085	1093	1086	1062	1136	1145	1141	1154	1070	1095	1074	1107	-33	
	1	1078	1069	1073	1078	1070	1046	1095	1103	1106	1120	1057	1081	1074	1083	-9	1073° C
	2	1077	1069	1062	1064	1054	1030	1055	1063	1072	1088	1045	1067	1073	1060	13	1.4 wt.%
	3	1077	1069	1050	1049	1038	1015	1018	1026	1040	1057	1033	1054	1073	1038	35	
3	0	1079	1077	1085	1097	1092	1064	1141	1148	1148	1161	1074	1104	1078	1111	-33	
	1	1078	1077	1073	1082	1075	1047	1099	1106	1112	1126	1062	1089	1078	1087	-9	1077° C
	2	1077	1077	1062	1068	1059	1032	1060	1067	1078	1094	1049	1076	1077	1064	13	1.4 wt.%
	3	1077	1077	1050	1053	1043	1016	1022	1029	1046	1063	1037	1062	1077	1042	35	
4	0	1079	1085	1085	1101	1097	1065	1146	1152	1154	1167	1079	1112	1082	1116	-34	
	1	1078	1085	1073	1086	1080	1049	1104	1110	1119	1133	1066	1098	1081	1092	-11	1081° C
	2	1077	1085	1062	1072	1064	1033	1064	1070	1084	1100	1054	1084	1081	1069	12	1.5 wt.%
	3	1077	1085	1050	1057	1049	1018	1027	1032	1052	1068	1042	1070	1081	1046	35	

[1]Numbers correspond to equation numbers from Putirka (2008). Phases on which thermometers are based: 13-16 = liquid only; 21-22 = olivine-liquid; 23-26 = plagioclase-liquid; 33-34 = clinopyroxene-liquid

[2]T-H_2O conditions (for a given pressure) at which the thermometers with and without an H_2O term converge

Table 6 Rb-Ba fractional vs. equilibrium crystallization model

	Mineral-Melt Partition Coefficients[1]						
	Ol	Opx	Cpx	Plag	Amph	Ox	Ap
Rb	0.01	0.02	0.03	0.02	0.29	0	0.3
Ba	0.01	0.02	0.03	See text	0.42	0	0.4

Fractionating assemblage[2]	
0-45% solid	0.53 plag + 0.27 cpx + 0.04 ol + 0.15 ox + 0.01 ap
45-70% solid	0.7 plag + 0.15 opx + 0.05 cpx + 0.08 ox + 0.02 ap
70-85% solid	0.7 plag + 0.1 amph + 0.1 cpx + 0.08 ox + 0.02 ap

Ol = olivine; *opx* = orthopyroxene; *cpx* = clinopyroxene; *plag* = plagioclase; *amph* = amphibole; *ox* = FeTi oxide; *ap* = apatite.

[1]All partition coefficients are from Rollinson (1993) except ap-melt (poorly constrained) from the GERM database (earthref.org/GERM) and plag-melt for Ba from Blundy & Wood (1991; see text)

[2]Fractionating assemblages are estimated from pumice compositions, experiments and the estimate that opx-out and amph-in occur after ~70% crystallization

Table 7 Inputs and results of crystallization model for high-Na trend

	Starting liquid (692Ja)	Target liquid (271Jc)	Phase Compositions[1]					Bulk crystal composition	Model-reproduced Starting liquid	Crystal proportions (by mass)	
			Plag	Cpx	Ol	Ox 1	Ox 2[2]				
SiO_2	55.9	60.4	54.7	49.1	36.9	0.18	0.11	44.4	55.7		
TiO_2	2.16	1.55		1.75	0.13	22.0	45.1	3.88	2.34	**Plag :**	**54.3**
Al_2O_3	16.1	16.0	27.7	3.88		2.5	0.48	16.5	16.2	**Cpx:**	**27.4**
FeO	9.48	6.95	1.03	11.0	27.6	72.8	48.2	15.4	9.03	**Ol:**	**3.1**
MgO	3.22	2.33	0.11	14.9	35.1	2.51	6.11	5.62	3.38	**Ox 1:**	**14.9**
CaO	6.65	4.89	10.9	18.9	0.27			11.1	6.67	**Ox 2:**	**0.3**
Na_2O	4.79	5.59	5.46	0.41				3.08	5.09		
K_2O	1.01	1.36	0.14					0.08	1.03		

[1]Phase compositions are those of phenocryst phases in sample 692Ja as determined by electron microprobe

[2]Oxide 2 comes from the 1 kbar experimental run 692Ja-43 because no Ti-rich oxide was found as a phenocryst in 692Ja

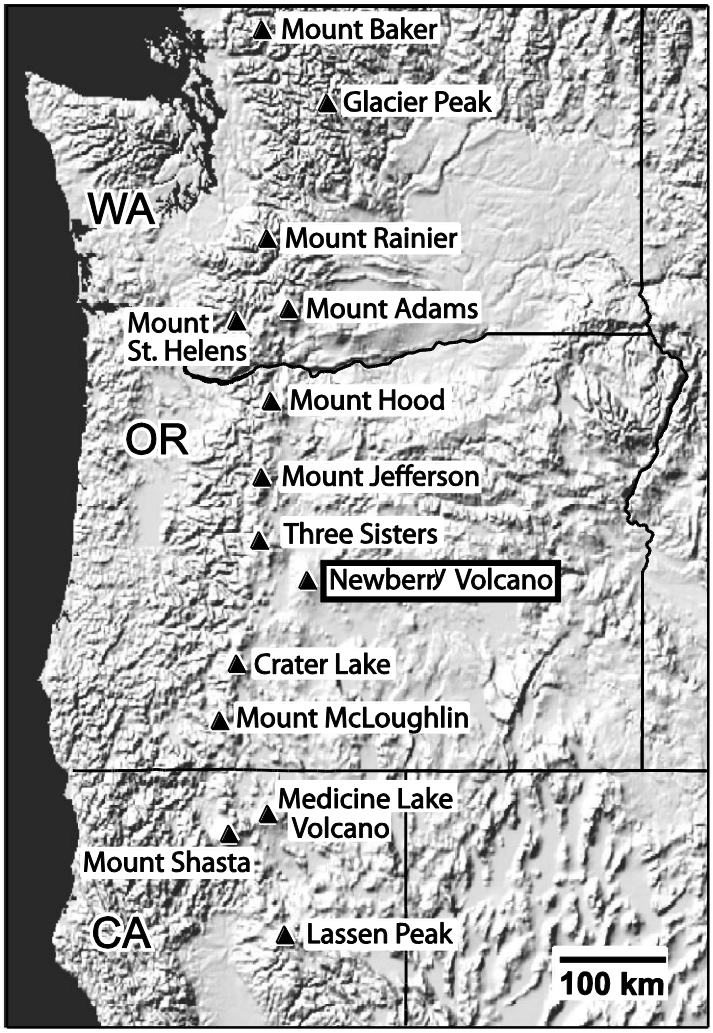
Mount Baker
Glacier Peak
WA
Mount Rainier
Mount Adams
Mount
St. Helens
Mount Hood
OR
Mount Jefferson
Three Sisters
Newberry Volcano
Crater Lake
Mount McLoughlin
Medicine Lake
Volcano
Mount Shasta
CA
Lassen Peak
100 km

Figure 1

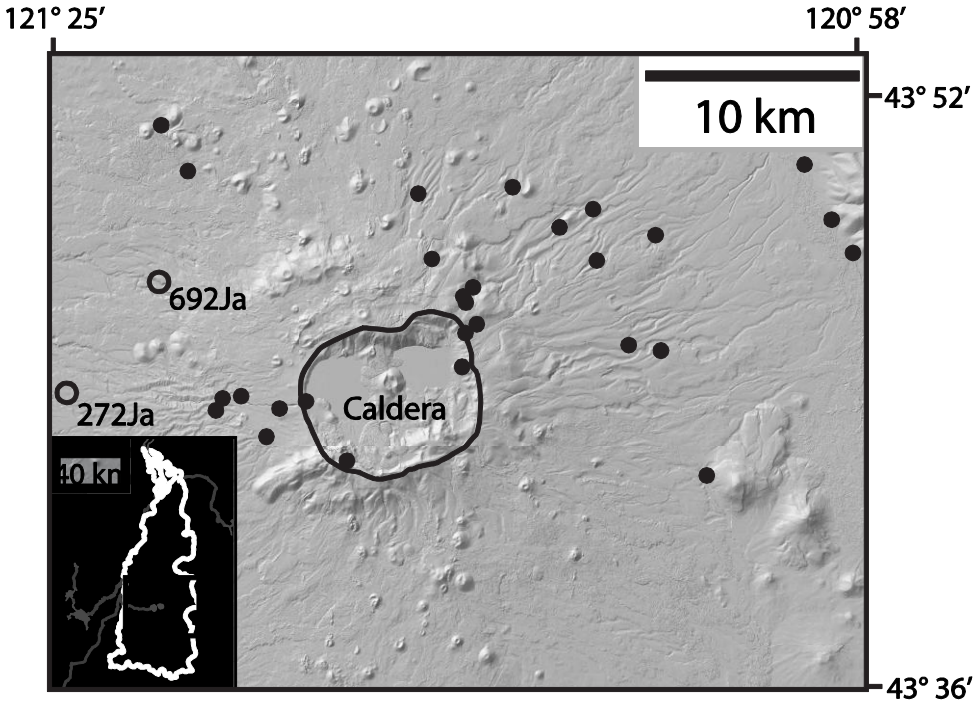

Figure 2

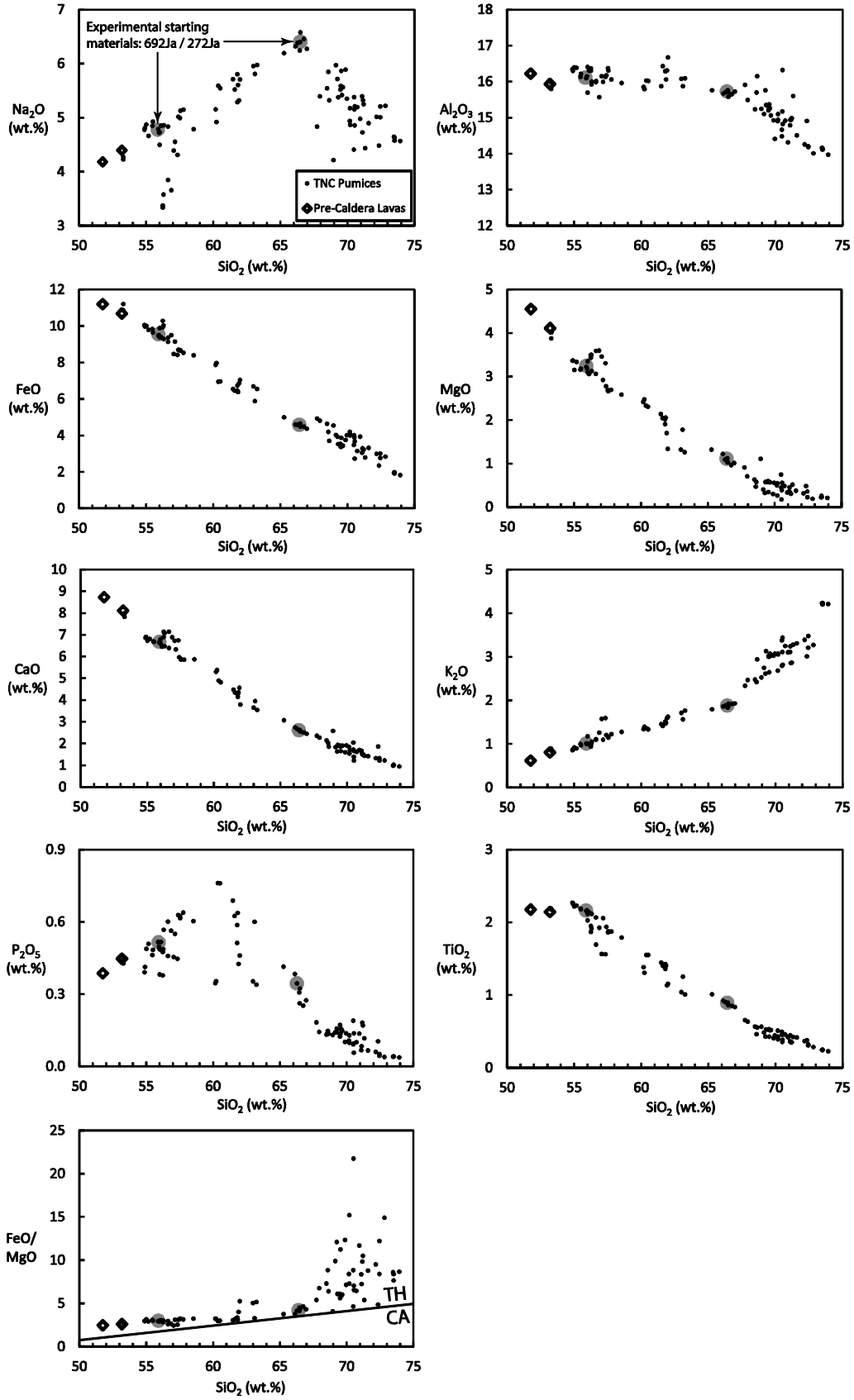
Experimental starting materials: 692Ja / 272Ja
TNC Pumices
Pre-Caldera Lavas
Na2O (wt.%)
Al2O3 (wt.%)
FeO (wt.%)
MgO (wt.%)
CaO (wt.%)
K2O (wt.%)
P2O5 (wt.%)
TiO2 (wt.%)
FeO/MgO
TH
CA
SiO2 (wt.%)

Figure 3

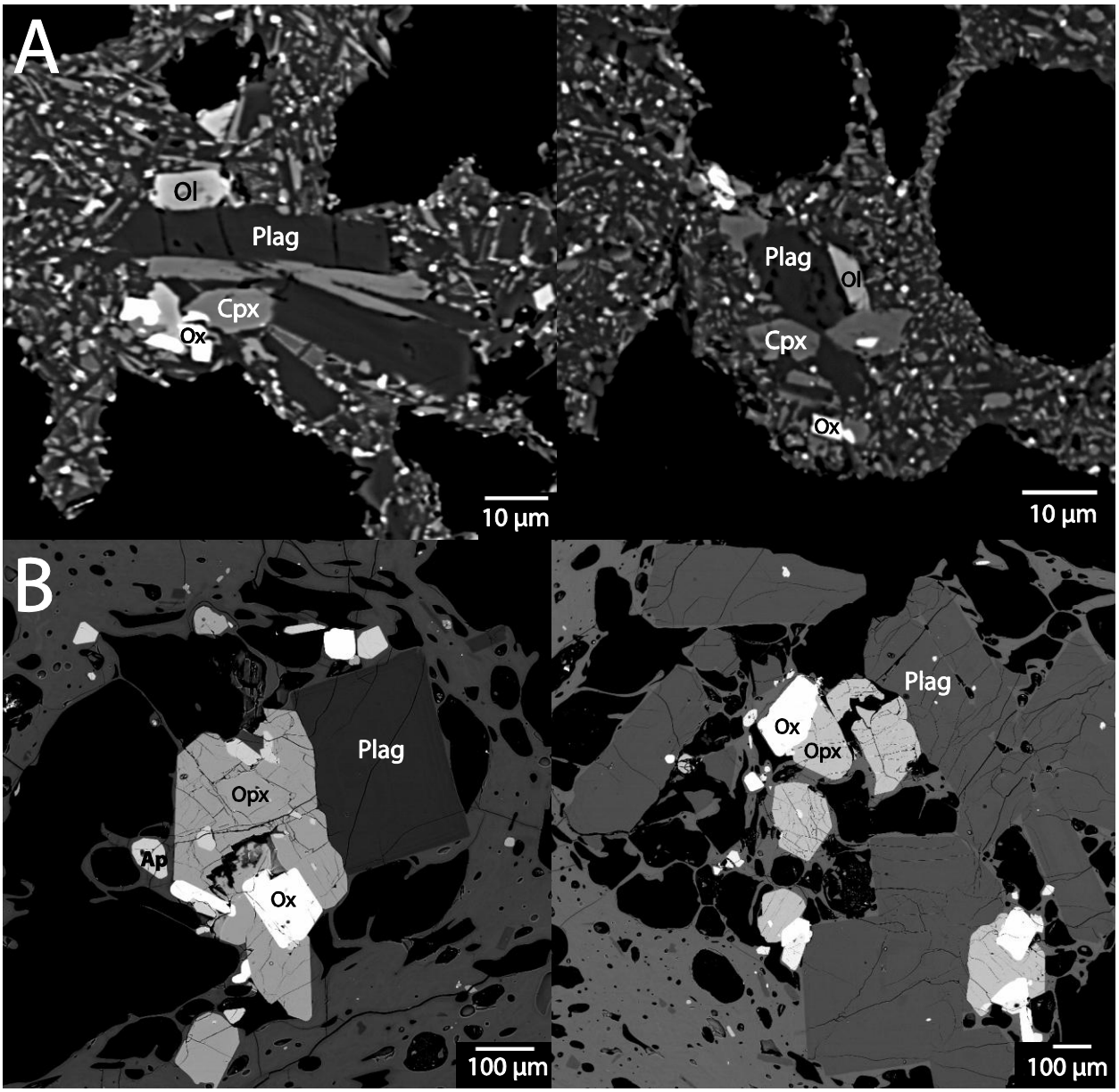
A
Ol
Plag
Cpx
Ox
10 µm
Plag
Ol
Cpx
Ox
10 µm
B
Plag
Opx
Ap
Ox
100 µm
Plag
Ox
Opx
100 µm

Figure 4

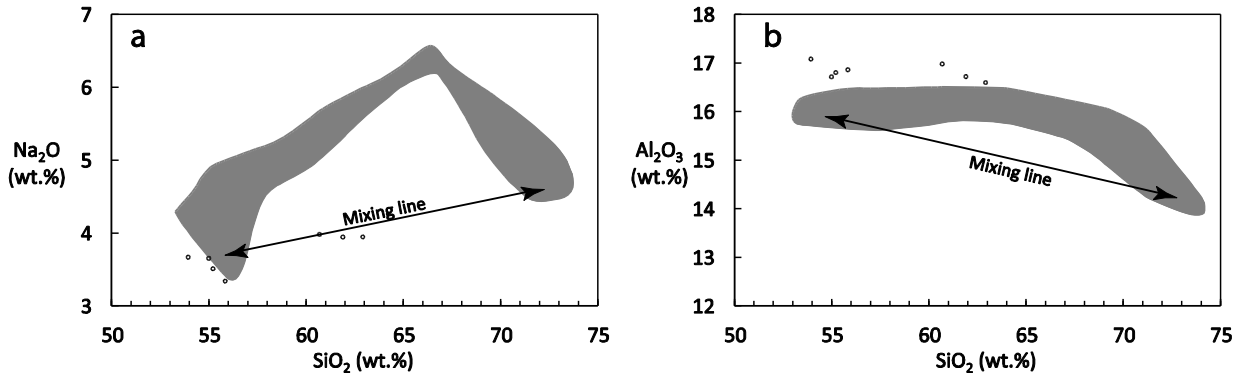
a
b
Na2O (wt.%)
Al2O3 (wt.%)
SiO2 (wt.%)
SiO2 (wt.%)
Mixing line
Mixing line
7
6
5
4
3
18
17
16
15
14
13
12
50
55
60
65
70
75

Figure 5

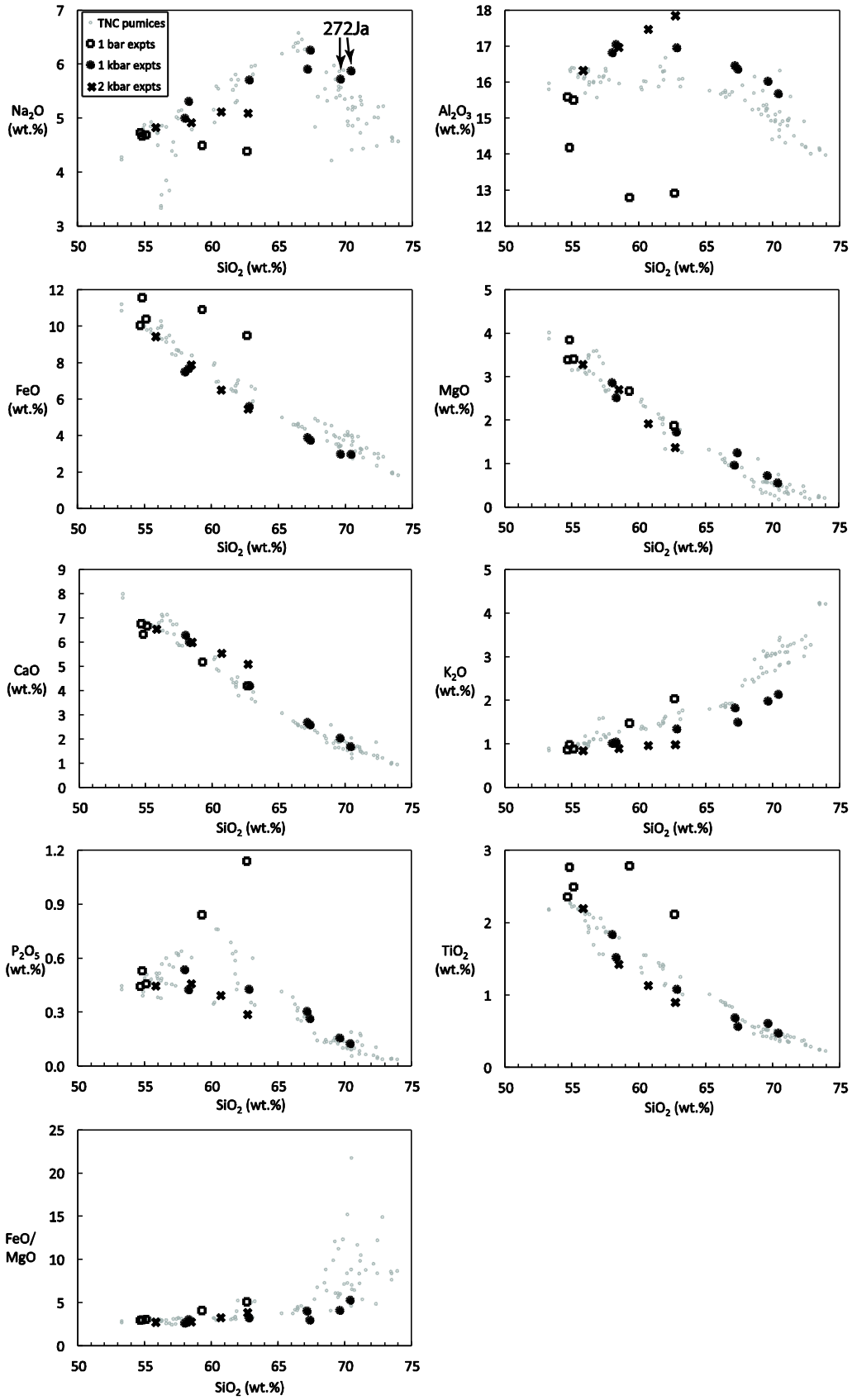
TNC pumices
1 bar expts
1 kbar expts
2 kbar expts
272Ja
Na2O (wt.%)
Al2O3 (wt.%)
FeO (wt.%)
MgO (wt.%)
CaO (wt.%)
K2O (wt.%)
P2O5 (wt.%)
TiO2 (wt.%)
FeO/MgO
SiO2 (wt.%)

Figure 6

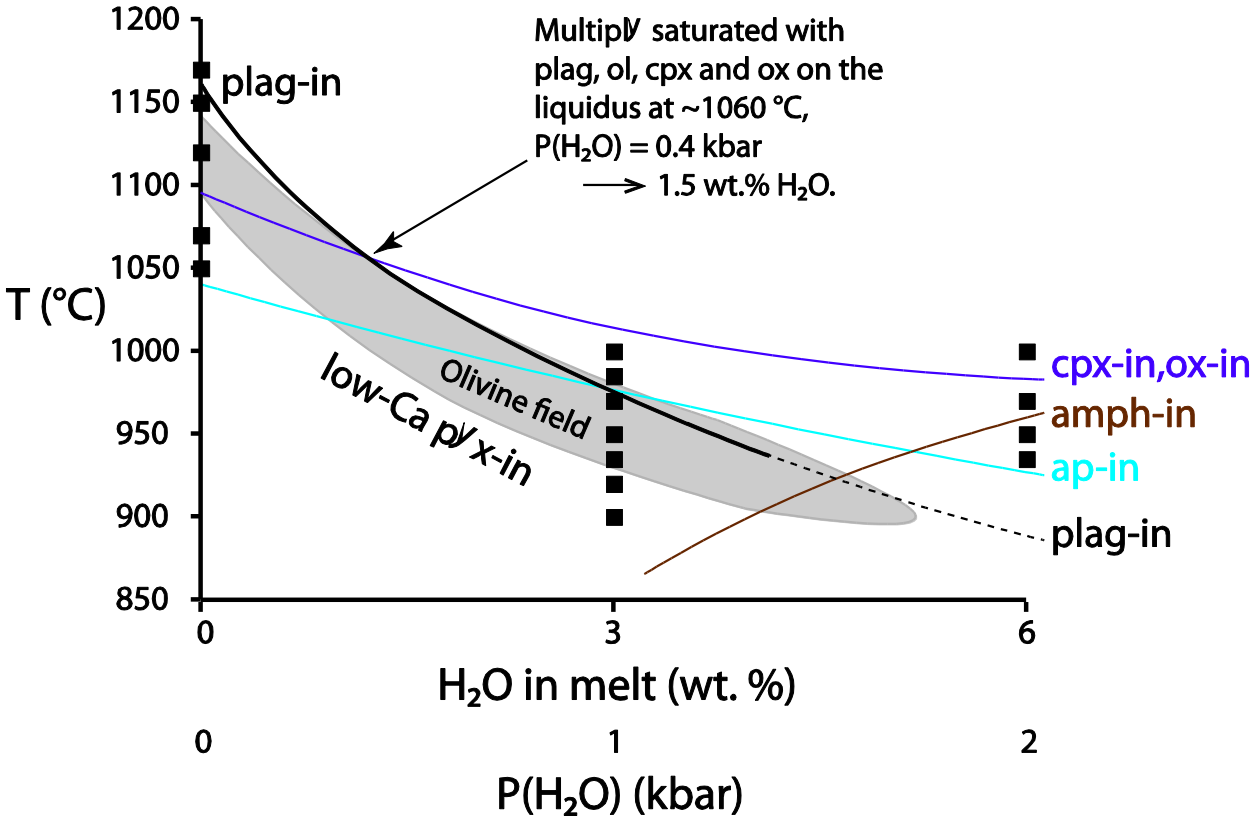
1200
1150
1100
1050
1000
950
900
850
T (°C)
plag-in
Multiply saturated with
plag, ol, cpx and ox on the
liquidus at ~1060 °C,
P(H2O) = 0.4 kbar
→ 1.5 wt.% H2O.
Olivine field
low-Ca pyx-in
cpx-in,ox-in
amph-in
ap-in
plag-in
0
3
6
H2O in melt (wt. %)
0
1
2
P(H2O) (kbar)

Figure 7

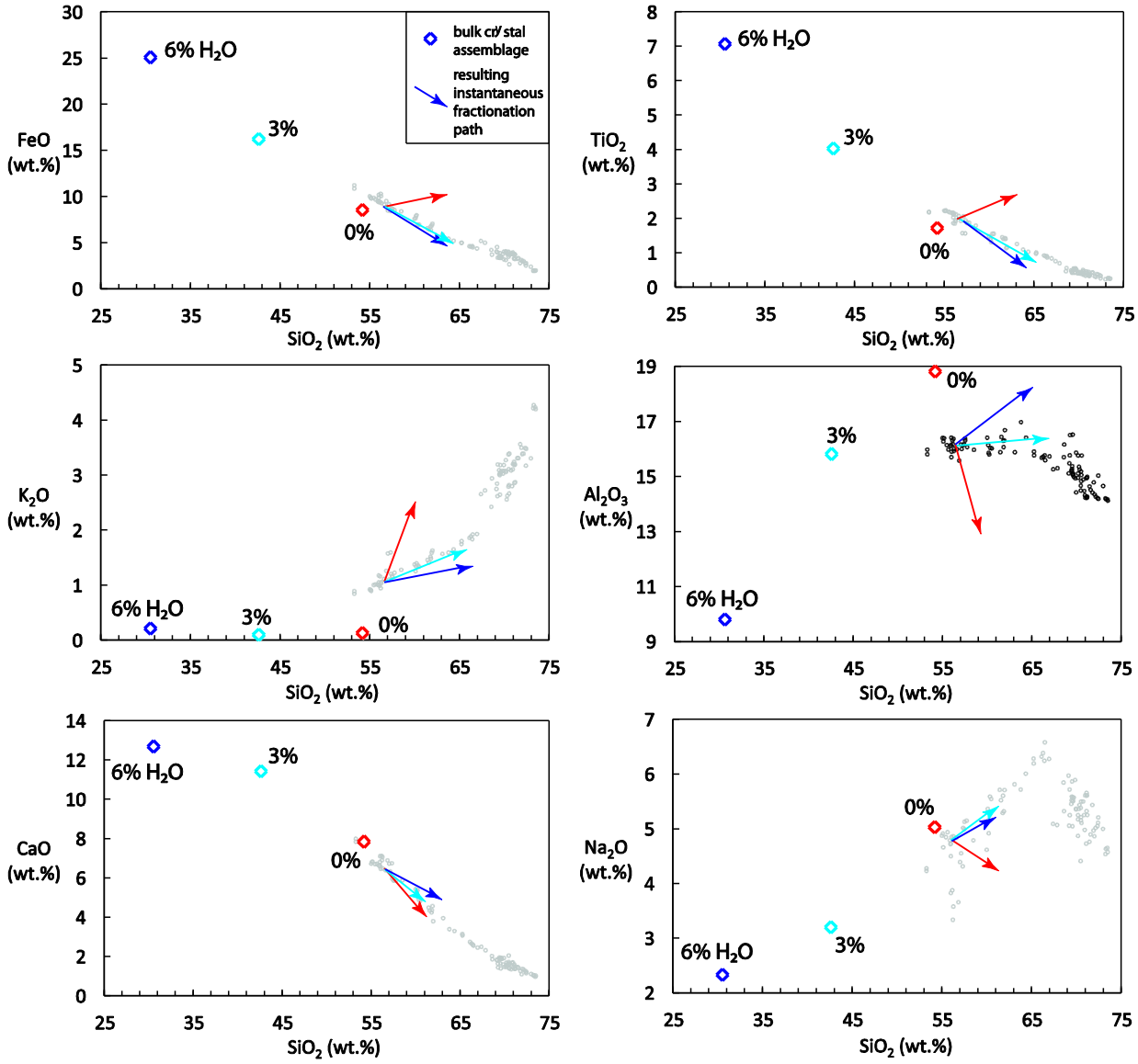
bulk crystal assemblage
resulting instantaneous fractionation path
FeO (wt.%)
TiO2 (wt.%)
K2O (wt.%)
Al2O3 (wt.%)
CaO (wt.%)
Na2O (wt.%)
SiO2 (wt.%)
6% H2O
3%
0%

Figure 8

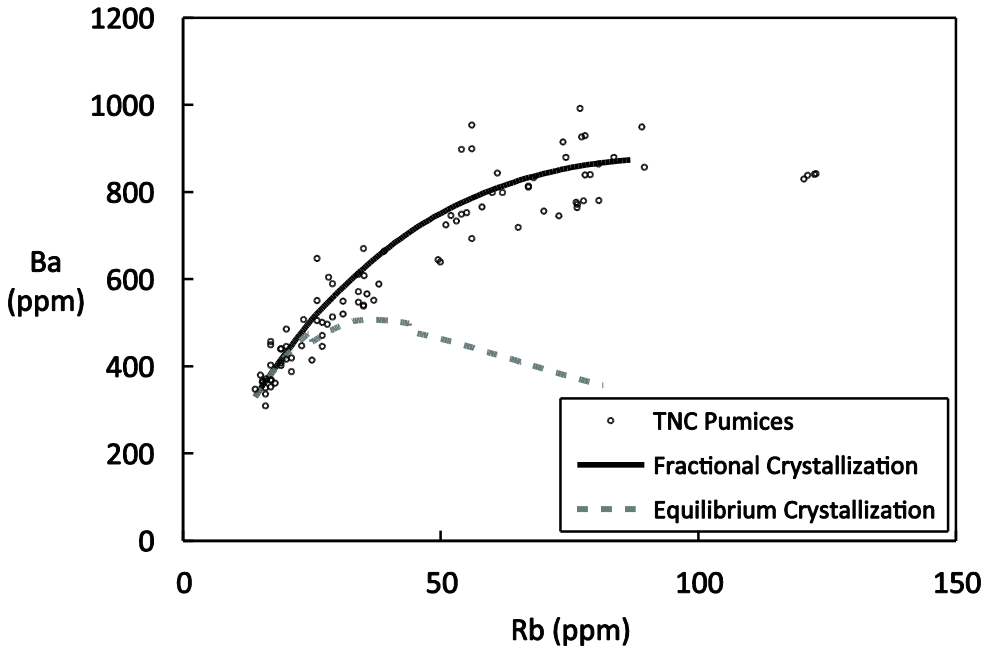
1200
1000
800
600
400
200
0
Ba
(ppm)
0
50
100
150
Rb (ppm)
TNC Pumices
Fractional Crystallization
Equilibrium Crystallization

Figure 9

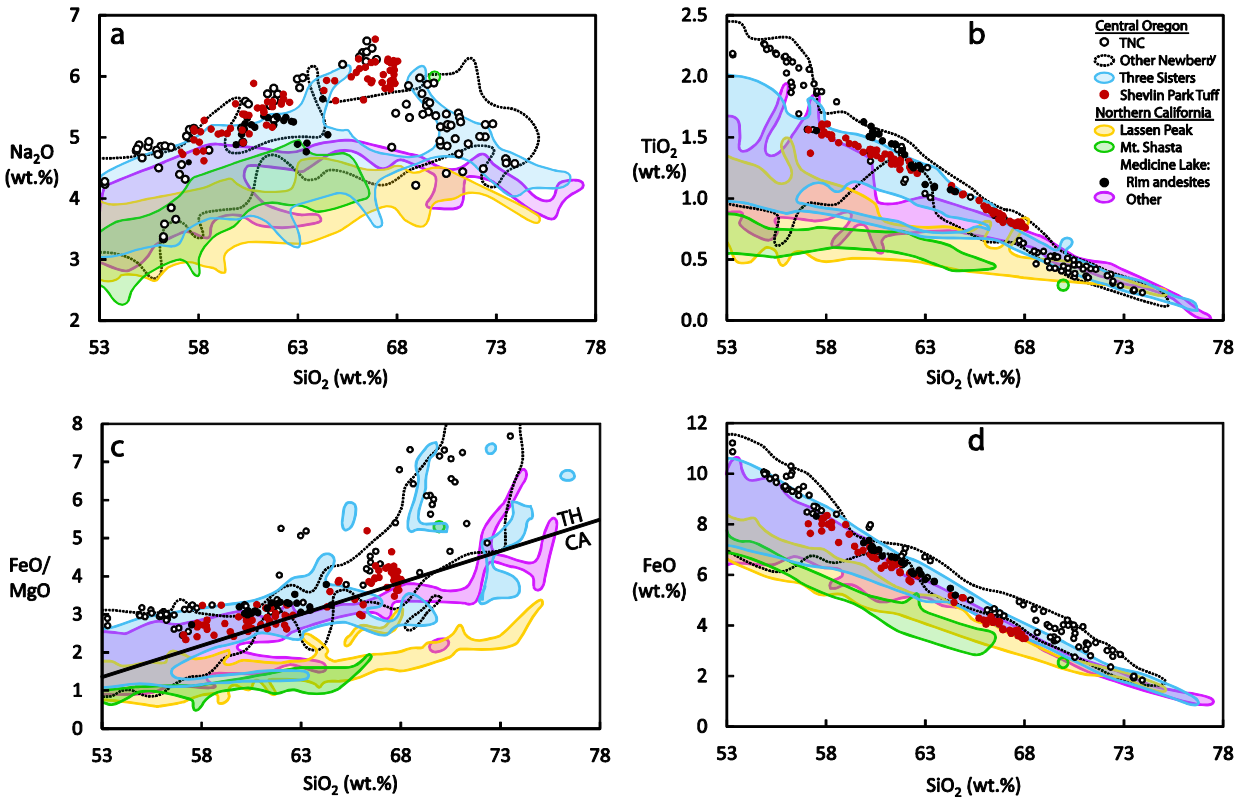
a
b
c
d
Na2O (wt.%)
TiO2 (wt.%)
FeO/ MgO
FeO (wt.%)
SiO2 (wt.%)
Central Oregon
TNC
Other Newberry
Three Sisters
Shevlin Park Tuff
Northern California
Lassen Peak
Mt. Shasta
Medicine Lake:
Rim andesites
Other
TH
CA

Figure 10